Geological Society of America Bulletin

$^{40}Ar/^{39}Ar$ chronostratigraphy of Altiplano-Puna volcanic complex ignimbrites reveals the development of a major magmatic province

Morgan J. Salisbury, Brian R. Jicha, Shanaka L. de Silva, Brad S. Singer, Néstor C. Jiménez and Michael H. Ort

Geological Society of America Bulletin 2011;123, no. 5-6;821-840
doi: 10.1130/B30280.1

Notes

$^{40}Ar/^{39}Ar$ chronostratigraphy of Altiplano-Puna volcanic complex ignimbrites reveals the development of a major magmatic province

Morgan J. Salisbury[1,†], Brian R. Jicha[2], Shanaka L. de Silva[1], Brad S. Singer[2], Néstor C. Jiménez[3], and Michael H. Ort[4]

[1]*Department of Geosciences, Oregon State University, Corvallis, Oregon 97331, USA*
[2]*Department of Geoscience, University of Wisconsin–Madison, Madison, Wisconsin 53706, USA*
[3]*Instituto de Investigaciones Geológicas y del Medio Ambiente, Universidad Mayor de San Andrés, La Paz, Bolivia*
[4]*School of Earth Sciences and Environmental Sustainability, Northern Arizona University, Flagstaff, Arizona 86011, USA*

ABSTRACT

The Lípez region of southwest Bolivia is the locus of a major Neogene ignimbrite flare-up, and yet it is the least studied portion of the Altiplano-Puna volcanic complex of the Central Andes. Recent mapping and laser-fusion $^{40}Ar/^{39}Ar$ dating of sanidine and biotite from 56 locations, coupled with paleomagnetic data, refine the timing and volumes of ignimbrite emplacement in Bolivia and northern Chile to reveal that monotonous intermediate volcanism was prodigious and episodic throughout the complex. The new results unravel the eruptive history of the Pastos Grandes and Guacha calderas, two large multicyclic caldera complexes located in Bolivia. These two calderas, together with the Vilama and La Pacana caldera complexes and smaller ignimbrite shields, were the dominant sources of the ignimbrite-producing eruptions during the ~10 m.y. history of the Altiplano-Puna volcanic complex. The oldest ignimbrites erupted between 11 and 10 Ma represent relatively small volumes (approximately hundreds of km^3) of magma from sources distributed throughout the volcanic complex. The first major pulse was manifest at 8.41 Ma and 8.33 Ma as the Vilama and Sifon ignimbrites, respectively. During pulse 1, at least 2400 km^3 of dacitic magma was erupted over 0.08 m.y. Pulse 2 involved near-coincident eruptions from three of the major calderas resulting in the 5.60 Ma Pujsa, 5.65 Ma Guacha, and 5.45 Ma Chuhuilla ignimbrites, for a total minimum volume of 3000 km^3 of magma. Pulse 3, the largest, produced at least 3100 km^3 of magma during a 0.1 m.y. period centered at 4 Ma, with the eruption of the 4.09 Ma Puripicar, 4.00 Ma Chaxas, and 3.96 Ma Atana ignimbrites. This third pulse was followed by two more volcanic explosivity index (VEI) 8 eruptions, producing the 3.49 Ma Tara (800 km^3 dense rock equivalent [DRE]) and 2.89 Ma Pastos Grandes (1500 km^3 DRE) ignimbrites. In addition to these large caldera-related eruptions, new age determinations refine the timing of two little-known ignimbrite shields, the 5.23 Ma Alota and 1.98 Ma Laguna Colorada centers. Moreover, $^{40}Ar/^{39}Ar$ age determinations of 13 ignimbrites from northern Chile previously dated by the K-Ar method improve the overall temporal resolution of Altiplano-Puna volcanic complex development. Together with the updated volume estimates, the new age determinations demonstrate a distinct onset of Altiplano-Puna volcanic complex ignimbrite volcanism with modest output rates, an episodic middle phase with the highest eruption rates, followed by a decline in volcanic output. The cyclic nature of individual caldera complexes and the spatiotemporal pattern of the volcanic field as a whole are consistent with both incremental construction of plutons as well as a composite Cordilleran batholith.

INTRODUCTION

The Altiplano-Puna volcanic complex (de Silva, 1989a) of the Central Andes is one of the world's premier settings for studying large silicic volcanism and its relation to plutonic underpinnings. The hyperarid climate of the Altiplano-Puna region during the past several million years has resulted in excellent preservation of Altiplano-Puna volcanic complex ignimbrites, but it has also limited erosion and vertical exposure, thereby hampering the establishment of a regional stratigraphy based on physical characteristics of successive ignimbrites. Although this region includes some of the world's largest documented ignimbrite eruptions (Guest, 1969; de Silva, 1989b) including the Atana (Gardeweg and Ramírez, 1987; Lindsay et al., 2001a), Puripicar (de Silva and Francis, 1989), and Vilama (Soler et al., 2007) ignimbrites, many fundamental stratigraphic details of the volcanic field remain to be understood. A conspicuous gap in the knowledge of the regional ignimbrites lies within the Lípez region of southwest Bolivia, in the heart of the Altiplano-Puna volcanic complex, where we have concentrated our study and sufficient exposure of basement allows us to define the onset of the major ignimbrite volcanism. We report new geologic mapping, precise $^{40}Ar/^{39}Ar$ age determinations from 56 sites in Bolivia and Chile, geochemical analyses, and volume calculations of, until now, little-studied ignimbrites and eruptive centers including the large Pastos Grandes and Guacha caldera complexes. The 13 $^{40}Ar/^{39}Ar$ sample sites in northern Chile were previously described and K-Ar dated by de Silva (1989b). Additionally, we incorporate $^{40}Ar/^{39}Ar$ ages determined for five Altiplano-Puna volcanic complex ignimbrites in Chile reported by Barquero-Molina (2003). Using these data, we reveal in detail the development of one of the world's youngest and best-preserved large silicic volcanic fields. This contribution to Altiplano-Puna volcanic complex volcanism includes new estimates of (1) the spatial extent of individual ignimbrites, (2) rates of volcanic fluxes and pulses, and (3) the longevity and repose periods of multicyclic nested caldera systems. We in turn examine the underlying causes of the Altiplano-Puna volcanic complex ignimbrite flare-up and the assembly of individual plutonic centers and Cordilleran batholiths.

†E-mail: salisbum@geo.oregonstate.edu

GSA Bulletin; May/June 2011; v. 123; no. 5/6; p. 821–840; doi: 10.1130/B30280.1; 10 figures; 6 tables; Data Repository item 2011016.

GEOLOGICAL CONTEXT—THE ALTIPLANO-PUNA VOLCANIC COMPLEX

The Altiplano-Puna plateau of the Central Andes is second only to the Tibetan Plateau in terms of areal extent, elevation, and crustal thickness. Unlike Tibet, however, the Altiplano-Puna plateau was formed at an active continental margin characterized by subduction of a dense oceanic plate (Nazca) beneath old, continental lithosphere (Brazilian craton of the South American plate). Thus, the plateau is the only modern region of its size and character to also involve subduction-zone magmatism. Subduction zone volcanism has been active in the Central Andes since the Jurassic, and significant tectonic shortening has occurred throughout the Cenozoic with major uplift of the plateau in the Late Cenozoic. Crustal shortening resulted in the presently thick continental crust (up to 70 km) beneath the Altiplano-Puna Plateau. After a hiatus related to flat-slab subduction, volcanism in the Altiplano-Puna plateau was abruptly widespread at ca. 27 Ma and may be related to delamination of the lower lithosphere (see Kay and Coira, 2009). The large crustal thicknesses have resulted in severe contamination of nearly all Central Andean arc magmas that postdate crustal shortening (Davidson et al., 1991; Davidson and de Silva, 1992; Wörner et al., 1994). The most significant crustal contributions to mantle-derived magmas occur in the Altiplano-Puna volcanic complex at the intersection between the Altiplano and Puna regions of the plateau (Fig. 1). The intense ignimbrite flare-up began in the mid-Miocene and occurs in a region of ~70,000 km^2 (21°S–24°S) east of the active arc front where base elevations are in excess of 4 km, the highest of the plateau. A seismically imaged low-velocity layer that has been interpreted to contain significant amounts of partial melt (Chmielowski et al., 1999; Zandt et al., 2003) underlies the comlex. The ignimbrites of the Altiplano-Puna volcanic complex are of the "monotonous intermediate" variety (Hildreth, 1981), are dominantly calc-alkaline, high-K dacites with minor rhyolite, and are thought to be erupted portions of a major Cordilleran batholith that underpins the Altiplano-Puna volcanic complex (de Silva et al., 2006a, 2006b; de Silva and Gosnold, 2007).

The ignimbrite sheets typically contain large (up to 5 mm) phenocrysts of plagioclase, quartz, biotite, amphibole, and Fe-Ti oxides with occasional sanidine, along with ubiquitous apatite, titanite, and zircon. Isotopic and other geochemical constraints of individual centers suggest assimilation of 50%–70% crust by mantle-derived magmas (de Silva, 1989a; Ort et al., 1996; Lindsay et al., 2001b; Schmitt et al., 2001). Large dacitic ignimbrite sheets are typically associated with equally impressive caldera dimensions, commonly in excess of 45 km in diameter. In the Altiplano-Puna volcanic complex, at least seven eruptions related to four caldera complexes with large resurgent centers (Pastos Grandes, Guacha, Vilama, La Pacana) are classified as 8 or greater on the volcanic explosivity index (VEI; Newhall and Self, 1982). Such eruptions are commonly referred to as supereruptions with dense rock equivalent (DRE) volumes in excess of 450 km^3 (Sparks et al., 2005; Self, 2006). Additionally, the Altiplano-Puna volcanic complex contains numerous lesser-volume ignimbrite shields that are apparently unrelated to major caldera collapse and resurgence. Our new spatiotemporal and compositional data further the understanding of the size and eruptive loci of the Altiplano-Puna volcanic complex ignimbrites and the development of abundant silicic magmatism in this region.

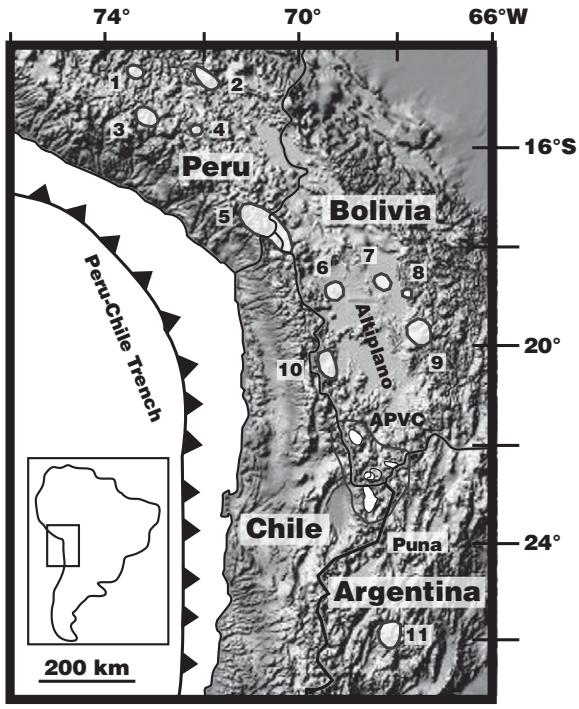

Figure 1. Location map of the Altiplano-Puna volcanic complex (APVC) and known Neogene ignimbrite eruptive centers of the Central Andes. Major calderas within the extent of Altiplano-Puna volcanic complex ignimbrites are outlined. Ignimbrite centers: 1—Cailloma, 2—Macusani, 3—Arequipa, 4—Salas, 5—Mauri-Lauca, 6—Curahuara, 7—Soledad, 8—Morococala, 9—Frailes, 10—Empexa, 11—Galán. Inset shows location of map along the western edge of South America.

METHODS

Sample Collection and Field Mapping

With the goal of establishing the spatiotemporal development of the Altiplano-Puna volcanic complex, our two primary objectives of this work were to identify and correlate individual ignimbrites and to establish a coherent stratigraphic framework throughout the region. Our work in the La Pacana caldera to the south (Lindsay et al., 2001a), Panizos on the eastern edge of the Altiplano-Puna volcanic complex (Ort, 1993), and the western flank of the Altiplano-Puna volcanic complex (de Silva, 1989b) provides detailed stratigraphy that can be extended into the study area in Bolivia. The presence of basement outcrops in areas like the Quetena valley and in the eastern margin of the Altiplano-Puna volcanic complex allowed fiduciary stratigraphic sections to be identified. Continuity of outcrop and sufficient vertical exposure allowed a coherent stratigraphy of the largest ignimbrites to be developed throughout the region. For instance, the Vilama (Soler et al., 2007), and now the Guacha ignimbrites, can be traced throughout a large part of the study area, and their basal and upper contacts are clear in many areas. The newly defined Tara and Pastos Grandes ignimbrites are the youngest major ignimbrites in the area and are consequently well exposed for much of their extent. The most difficult correlations occur on the edges of the ignimbrite plateau, in areas of Quaternary volcanism close to the active arc, and distal outliers without clear stratigraphic context. Sampling therefore focused on distal outcrops as well as key stratigraphic sections throughout the plateau. Juvenile pumice blocks were sampled from the ignimbrites wherever possible to avoid possible xenocrystic contamination; otherwise bulk ignimbrite was collected.

$^{40}Ar/^{39}Ar$ Geochronology

Samples of pumice, ignimbrite matrix (removed of obvious lithics), and lava were crushed with mortar and pestle, sieved to isolate 250–500 and 500–1000 μm size fractions, and rinsed in deionized water to remove vesicular glass. Euhedral biotite crystals were picked under a binocular microscope. Select biotite crystals were ultrasonically cleaned for 1 min in dilute (5%) nitric acid to remove adhering glass. Feldspar and quartz were concentrated using a Frantz magnetic separator. Sanidine crystals were largely isolated from the quartz and plagioclase using Na-polytungstate at 2.61 g/cm^3. Individual sanidine crystals were further distinguished via scanning electron microscopy (SEM) using energy dispersive spectrometry (EDS) at both Oregon State University and the University of Wisconsin–Madison. As a final purification step, sanidine crystals were cleaned ultrasonically in dilute (5%) hydrofluoric acid (HF) for 1 min followed by several rinses in deionized water.

Sanidine and biotite crystals from each sample were encapsulated in pure Al foil packets and placed into wells in 2.5-cm-diameter Al disks interspersed with 28.34 Ma sanidine from the Taylor Creek rhyolite (Renne et al., 1998) as a neutron flux monitor. The Al disks were irradiated for 3 h in the cadmium-lined in-core irradiation tube (CLICIT) at the Oregon State University TRIGA reactor. Based on previous experiments, corrections for undesirable nucleogenic reactions on ^{40}K and ^{40}Ca are as follows: $[^{40}Ar/^{39}Ar]_K = 0.00086$; $[^{36}Ar/^{37}Ar]_{Ca} = 0.000264$; and $[^{39}Ar/^{37}Ar]_{Ca} = 0.000673$ (Singer et al., 2004). Across individual Al disks, J values were uniform within a 2σ analytical uncertainty of 0.5%, which was propagated quadratically into the uncertainty on the final age of each sample.

At the University of Wisconsin–Madison Rare Gas Geochronology Laboratory, biotite and sanidine crystals were fused using a CO_2 laser at 25% and 35% output power, respectively. Single-crystal laser-fusion (SCLF) analyses were performed in most cases, although small biotites (<150 μm diameter) in some samples necessitated that multiple crystals be fused together to generate signals larger than blanks. Biotite was treated with a low-power (0.1 Watt) cleanup step using a defocused laser beam to release adsorbed loosely bound argon—largely atmospheric in composition—prior to total fusion. Fully automated experiments included fusion for 75 s, followed by gas cleanup on two SAES GP50 getters for either 180 s (sanidine) or 600 s (biotite). Blanks were measured frequently throughout the analytical sessions, typically after every two laser fusions. Isotopic analysis and data reduction followed the procedures of Smith et al. (2003). Mass discrimination, monitored using a pipette of atmospheric argon measured 108 times during the analytical sessions, varied by <±1.0‰ during each analytical session.

Paleomagnetism and Whole-Rock Geochemistry

Characteristic remanent magnetism (ChRM) directions and whole-rock geochemical analyses were performed to test correlations of various units that cover areas of up to several 1000 km^2 and to develop a database for future work. A summary of the paleomagnetic portion of this study (sampling, methods, and interpretation) is presented in Appendix 1, available through the GSA Data Repository.[1] A more comprehensive treatment will be published elsewhere. Because definitive textural, mineralogical, or geochemical fingerprints for individual ignimbrites are difficult to establish (de Silva and Francis, 1989), only limited whole-rock geochemical chemical analyses were conducted. Major- and trace-element analyses were performed by X-ray fluorescence (XRF) and inductively coupled plasma–mass spectrometry (ICP-MS) at GeoAnalytical Laboratories, Washington State University, Pullman, Washington (see Johnson et al., 1999).

Ignimbrite Correlation

We compiled a geographical information system (GIS) database containing our newly determined $^{40}Ar/^{39}Ar$ age determinations (Table 1) with the age and location of published isotopic ages determined for ignimbrites within the Altiplano-Puna volcanic complex. In addition, the GIS database includes the distributions of 300 ignimbrite outcrops of 60 units that were digitized from paper geologic maps of the Lípez region published by Servicio Nacional de Geología y Minería (SERGEOMIN, see references in Table 2). Field mapping and section logging during this study and over the last 20 yr, coupled with the new geochronologic data strongly suggested that the 60 individual ignimbrite units compiled in the Lípez region by SERGEOMIN represent a much smaller number of large-volume ignimbrites that, until now, could not be correlated owing to the lack of detailed study, and to the paucity and large uncertainties of previous age determinations. Work in northern Chile and elsewhere (de Silva and Francis, 1989; Hildreth and Mahood, 1985) has shown that large-volume ignimbrites (monotonous intermediates) are often difficult to distinguish in the field, and we used precise $^{40}Ar/^{39}Ar$ age determinations, in conjunction with field data and paleomagnetic signatures, to (1) correlate the previously mapped units by SERGEOMIN and others, (2) estimate the extent of each ignimbrite from the Lípez region of Bolivia, and (3) establish distinctive ages for the majority of Altiplano-Puna volcanic complex ignimbrites. We use our newly acquired geochemical data and the published age data within the database to support our conclusions and resolve complexities presented by the $^{40}Ar/^{39}Ar$ age data.

RESULTS

$^{40}Ar/^{39}Ar$ Age Determinations

The results of 848 single-crystal and 84 multicrystal fusion analyses from 60 samples are summarized in Table 1 (complete data in Appendix 2 [see footnote 1]). These new ages significantly expand and refine the geochronologic data available for the Altiplano-Puna volcanic complex. On average, 13 fusion ages were determined for each sample, and the results were pooled to calculate an inverse-variance weighted mean age. Because isochron regression of single- and multicrystal data revealed that excess argon is not present in either biotite or sanidine in a detectable amount, the weighted mean ages were taken to give the most precise estimates of time elapsed following eruption (Table 1). Sanidine analyses are preferred over biotite due to their large crystal size (>250 μm), higher K concentrations, higher precision, and potentially superior accuracy (e.g., Kelley, 2002; Hora et al., 2010). Sanidine data from 14 samples reveal Gaussian age distributions, with few outliers. Because sanidine was only present within some units (14 of the 60 samples analyzed), we rely on the weighted mean age of concordant biotite single-crystal fusion experiments as the best estimate for the eruption age of many units. In 10 samples, we analyzed both biotite and sanidine, and the sanidine $^{40}Ar/^{39}Ar$ ages were younger (and outside of 2σ error) in every case, with the exception of the two least precise biotite ages (B06-018 and B06-002), which overlapped the corresponding sanidine ages within 2σ error (Figs. 2 and 3). The offset between sanidine and biotite ages shows no systematic variation with younger or older ages and ranges from concordant up to 320 k.y.

[1]GSA Data Repository item 2011016, methodology and results of ChRM paleomagnetism; results of whole-rock chemical analyses; and full results of single-crystal and multiple-crystal, laser fusion $^{40}Ar/^{39}Ar$ analyses, is available at http://www.geosociety.org/pubs/ft2011.htm or by request to editing@geosociety.org.

TABLE 1. SUMMARY OF $^{40}Ar/^{39}Ar$ LASER FUSION ANALYSES

Sample no.	Map*	Mat†	Min§	Latitude (°S)	Longitude (°W)	$^{40}Ar/^{36}Ar_i$ (±2σ)	Isochron age (Ma, ±2σ)	MSWD#	Weighted mean age** (Ma, ±2σ)	MSWD	N
Age determinations from multiple ignimbrite samples											
Tatio ignimbrite											
B06-069	1	pum	bio	22.3013	67.7631	292.2 ± 05.6	0.72 ± 0.04	0.39	0.699 ± 0.01	0.45	14 of 14
B06-070	2	mat	bio	22.3438	67.7939	294.2 ± 07.1	0.77 ± 0.13	0.90	0.750 ± 0.06	0.81	10 of 10
B06-067	1	pum	bio	22.3007	67.7613	295.6 ± 09.1	0.76 ± 0.13	1.60	0.764 ± 0.06	1.40	10 of 10
							Weighted mean age of 34 analyses		**0.703 ± 0.010**	1.14	34
Laguna Colorada ignimbrite											
B06-062	3	mat	bio	22.2234	67.4256	278.0 ± 25.0	2.09 ± 0.21	0.95	1.95 ± 0.03	0.98	9 of 11
89022	4	mat	bio	22.1857	67.5154	295.9 ± 16.2	2.04 ± 0.22	0.58	2.05 ± 0.05	0.54	14 of 14
							Weighted mean age of 23 analyses		**1.98 ± 0.03**	1.30	23
Pastos Grandes ignimbrite											
89017	5	mat	bio	21.8182	67.8280	306.0 ± 13.0	2.86 ± 0.08	0.51	2.91 ± 0.03	0.63	14 of 14
B06-036	6	mat	bio	21.5958	67.6083	299.0 ± 38.0	8.40 ± 0.18	0.15	2.93 ± 0.01	0.60	12 of 12
B06-056	7	mat	bio	21.6550	67.7303	296.9 ± 05.5	2.95 ± 0.05	1.17	2.96 ± 0.02	0.53	11 of 12
B06-058	8	mat	bio	21.9443	67.8738	310.0 ± 33.0	2.92 ± 0.11	0.65	2.97 ± 0.02	0.63	12 of 12
							Weighted mean age of 49 analyses		2.94 ± 0.01	0.88	49
B06-056	7	mat	san	21.6550	67.7303	293.0 ± 18.0	2.89 ± 0.02	1.06	2.88 ± 0.01	0.65	17 of 17
B06-058	8	mat	san	21.9443	67.8738	294.0 ± 37.0	2.88 ± 0.02	0.66	2.88 ± 0.01	0.44	14 of 14
B06-036	6	mat	san	21.5958	67.6083	292.1 ± 06.2	2.95 ± 0.03	0.70	2.89 ± 0.01	0.75	18 of 18
B06-045	9	mat	san	21.4346	67.6374	293.0 ± 15.0	2.91 ± 0.02	0.89	2.91 ± 0.02	0.77	17 of 19
							Weighted mean age of 66 analyses		**2.89 ± 0.01**	0.78	66
Tara ignimbrite											
B06-081	10	pum	bio	22.4388	67.3760	295.4 ± 01.2	3.87 ± 0.10	1.16	*3.86 ± 0.05*	*1.02*	*11 of 13*
B06-027	11	pum	bio	22.5012	67.4764	296.1 ± 04.1	3.88 ± 0.12	0.22	*3.89 ± 0.07*	*0.19*	*6 of 12*
B06-072	12	mat	bio	22.7550	67.6397	300.0 ± 12.0	3.44 ± 0.10	0.53	3.48 ± 0.03	0.52	13 of 13
B06-025	13	mat	bio	22.6331	67.4980	296.1 ± 30.0	3.55 ± 0.05	0.48	3.56 ± 0.02	0.40	13 of 13
B06-018	14	mat	bio	22.7756	67.2529	301.0 ± 16.0	3.51 ± 0.17	0.04	3.56 ± 0.07	0.13	6 of 6
B06-013	15	pum	bio	22.4479	67.2805	253.0 ± 76.0	3.69 ± 0.11	0.18	3.63 ± 0.04	0.24	6 of 6
							Weighted mean age of 38 analyses		3.55 ± 0.02	1.50	38
B06-018	14	mat	san	22.7756	67.2529	291.0 ± 14.0	3.51 ± 0.04	0.81	3.51 ± 0.01	0.56	32 of 32
89002	16	mat	san	22.5151	67.6409	295.0 ± 04.7	3.46 ± 0.03	1.37	3.46 ± 0.02	1.18	8 of 8
							Weighted mean age of 40 analyses		**3.49 ± 0.01**	1.17	40
Puripicar ignimbrite											
83015	17	pum	bio	22.70	68.24	294.8 ± 06.4	4.06 ± 0.13	1.50	4.05 ± 0.11	1.38	13 of 13
89001	18	mat	bio	22.3525	67.7278	301.5 ± 13.0	4.08 ± 0.05	1.20	4.09 ± 0.04	1.19	12 of 12
							Weighted mean age of 25 analyses		**4.09 ± 0.02**	1.13	25
Alota ignimbrite											
B06-063	19	pum	bio	21.4573	67.6457	247.0 ± 34.0	5.78 ± 0.13	0.61	5.63 ± 0.04	0.91	11 of 11
B06-063	19	pum	san	21.4573	67.6457	294.3 ± 02.5	5.25 ± 0.07	0.99	5.24 ± 0.02	0.40	23 of 27
ALI-189	20	pum	san	21.4809	67.6127	296.1 ± 10.5	5.22 ± 0.03	1.77	5.23 ± 0.02	1.56	9 of 9
							Weighted mean age of 32 analyses		**5.23 ± 0.01**	0.49	32
Chuhuilla ignimbrite											
89019b	21	mat	bio	21.7201	67.9552	292.9 ± 04.6	5.75 ± 0.11	0.89	*5.70 ± 0.03*	*0.78*	*10 of 10*
89019a	21	mat	bio	21.7201	67.9552	312.8 ± 20.2	5.11 ± 0.46	0.12	5.51 ± 0.03	0.78	4 of 4
B06-050	22	pum	bio	21.2490	68.1288	288.0 ± 12.0	5.60 ± 0.12	0.91	5.54 ± 0.03	0.55	12 of 12
							Weighted mean age of 16 analyses		5.52 ± 0.02	0.72	16
89019	21	mat	san	21.7201	67.9552	296.4 ± 06.4	5.45 ± 0.04	0.78	**5.45 ± 0.02**	0.46	16 of 17
Guacha ignimbrite											
B06-085	23	pum	bio	22.3545	67.3929	294.0 ± 01.8	5.73 ± 0.25	0.71	*5.52 ± 0.06*	*0.87*	*11 of 11*
B06-007	24	pum	bio	22.1630	67.3104	294.4 ± 02.5	5.92 ± 0.73	1.40	5.59 ± 0.19	1.30	12 of 12
B06-002	25	mat	bio	21.8401	67.3373	290.3 ± 06.4	5.80 ± 0.13	0.51	5.71 ± 0.05	0.62	12 of 12
B06-022	26	mat	bio	22.6085	67.3998	294.6 ± 02.8	5.78 ± 0.07	0.91	5.77 ± 0.04	0.61	10 of 12
B06-080	10	pum	bio	22.4388	67.3760	293.6 ± 03.7	5.81 ± 0.04	1.90	5.80 ± 0.00	1.04	13 of 12
B06-030	27	mat	bio	22.3813	67.1490	297.0 ± 10.0	5.82 ± 0.07	0.80	5.84 ± 0.02	0.50	12 of 12
							Weighted mean age of 59 analyses		5.81 ± 0.01	1.40	59
B06-002	25	mat	san	21.8401	67.3373	306.0 ± 45.0	5.65 ± 0.04	0.02	**5.65 ± 0.01**	0.52	26 of 26
Panizos ignimbrite											
BOL-07-005	28	pum	bio	22.2521	66.8351	294.0 ± 32.0	6.97 ± 0.25	1.70	*6.98 ± 0.04*	*1.50*	*12 of 12*
BOL-07-001	29	pum	bio	21.9834	66.5360	295.7 ± 02.9	6.66 ± 0.17	1.01	6.67 ± 0.07	0.90	12 of 12
BOL-07-002	30	pum	bio	22.0503	66.6334	301.0 ± 13.7	6.72 ± 0.07	0.29	6.75 ± 0.02	0.29	10 of 10
BOL-07-003	28	pum	bio	22.2521	66.8351	291.3 ± 04.6	6.78 ± 0.04	0.71	6.75 ± 0.02	0.83	12 of 12
BOL-07-004	28	pum	bio	22.2521	66.8351	293.3 ± 03.9	6.80 ± 0.06	0.77	6.78 ± 0.03	0.73	12 of 12
B06-077	31	pum	bio	22.1199	66.9163	293.0 ± 18.0	6.88 ± 0.15	1.12	6.86 ± 0.03	0.36	10 of 10
							Weighted mean age of 56 analyses		**6.79 ± 0.02**	2.50	56
Sifon ignimbrite											
83001	32	mat	bio	22.66	68.47	299.2 ± 28.0	8.20 ± 0.32	0.37	8.23 ± 0.15	0.35	14 of 14
83005	33	pum	bio	22.75	68.44	303.0 ± 23.6	8.28 ± 0.22	1.06	8.34 ± 0.07	1.02	14 of 14
							Weighted mean age of 28 analyses		**8.33 ± 0.06**	0.72	28

(*continued*)

TABLE 1. SUMMARY OF $^{40}Ar/^{39}Ar$ LASER FUSION ANALYSES (*continued*)

Sample no.	Map*	Mat†	Min§	Latitude (°S)	Longitude (°W)	$^{40}Ar/^{36}Ar_i$ (±2σ)	Isochron age (Ma, ±2σ)	MSWD#	Weighted mean age** (Ma, ±2σ)	MSWD	N
Age determinations from multiple ignimbrite samples (*continued*)											
Vilama ignimbrite											
B06-003	25	mat	bio	21.8410	67.3363	293.0 ± 03.9	8.30 ± 0.19	0.21	8.22 ± 0.11	0.32	12 of 12
B06-032	34	mat	bio	22.3414	67.1764	286.0 ± 17.0	8.41 ± 0.12	0.95	8.37 ± 0.04	0.49	12 of 12
B06-039	35	pum	bio	21.7250	67.3865	288.0 ± 28.0	8.44 ± 0.19	0.59	8.40 ± 0.05	0.17	6 of 6
B06-035	36	mat	bio	22.3916	66.9955	297.0 ± 13.0	8.42 ± 0.12	0.18	8.42 ± 0.04	0.08	12 of 12
B06-029	37	mat	bio	22.2506	67.3454	294.6 ± 03.2	8.42 ± 0.13	0.97	8.42 ± 0.05	0.51	12 of 12
B06-031	38	mat	bio	22.2265	67.0992	299.0 ± 38.0	8.40 ± 0.18	0.15	8.42 ± 0.06	7.16	12 of 12
B06-042	39	pum	bio	21.7173	67.3521	297.0 ± 16.0	8.46 ± 0.13	0.97	8.46 ± 0.04	0.42	11 of 12
						Weighted mean age of 77 analyses			**8.41 ± 0.02**	0.59	77
Artola ignimbrite											
83002††	32	mat	bio	22.66	68.47	303.8 ± 23.6	9.37 ± 0.22	0.87	9.45 ± 0.03	0.84	13 of 15
83028††	40	mat	bio	22.72	68.22	298.2 ± 20.9	9.32 ± 0.24	1.11	9.35 ± 0.03	1.04	15 of 15
						Weighted mean age of 28 analyses			**9.40 ± 0.03**	2.00	28
Ignimbrite ages from single samples											
Puripica Chico ignimbrite											
B06-073	41	pum	bio	22.6262	67.6788	297.1 ± 05.5	1.69 ± 0.06	0.67	**1.70 ± 0.02**	0.60	10 of 10
Talabre ignimbrite											
83078	42	mat	bio	23.59	67.88	304.4 ± 20.1	2.32 ± 0.40	0.80	**2.51 ± 0.08**	0.80	16 of 16
Atana ignimbrite											
83077	43	mat	bio	23.18	67.98	300.0 ± 13.5	3.92 ± 0.14	0.22	3.96 ± 0.08	0.24	13 of 13
Chaxas II ignimbrite											
83034	44	mat	bio	22.77	68.08	269.4 ± 33.8	4.12 ± 0.18	1.49	**4.00 ± 0.10**	1.65	10 of 12
Pelon ignimbrite											
83016††	17	mat	bio	22.70	68.24	290.4 ± 15.3	6.21 ± 1.11	0.83	**5.82 ± 0.08**	0.80	13 of 14
Linzor ignimbrite											
83065††	45	pum	bio	22.25	68.14	289.3 ± 09.4	6.51 ± 0.30	0.63	**6.33 ± 0.12**	0.70	15 of 15
Toconce ignimbrite											
83061	46	pum	bio	22.28	68.22	281.6 ± 23.2	6.84 ± 0.56	0.52	**6.52 ± 0.19**	0.57	15 of 15
Yerbas Buenas ignimbrite											
83022B††	47	mat	bio	22.66	68.23	311.7 ± 34.4	8.08 ± 0.45	0.72	**8.30 ± 0.04**	0.74	14 of 14
Chaxas I ignimbrite											
83035††	48	pum	bio	22.90	68.05	324.5 ± 51.8	8.13 ± 0.38	0.54	**8.35 ± 0.03**	0.61	14 of 14
Divisoco ignimbrite											
83050	49	mat	bio	22.28	68.29	299.7 ± 16.1	10.13 ± 0.22	0.81	**10.18 ± 0.15**	0.77	14 of 14
Rio San Antonio ignimbrite											
B06-005	50	pum	bio	22.1780	67.3123	304.0 ± 17.0	10.09 ± 0.83	0.41	**10.33 ± 0.64**	0.48	9 of 12
Lower Rio San Pedro ignimbrite											
83088	51	pum	bio	22.02	68.62	294.9 ± 6.7	10.72 ± 0.30	0.63	**10.71 ± 0.14**	0.58	16 of 16
Effusive eruptions											
Sombrero dome, Pastos Grandes caldera											
B06-057	52	lava	bio	21.7866	67.7534	296.6 ± 03.9	2.98 ± 0.06	1.20	3.00 ± 0.01	0.93	10 of 12
B06-057	52	lava	san	21.7866	67.7534	402.0 ± 280.0	2.80 ± 0.09	0.78	**2.83 ± 0.02**	0.75	13 of 14
Rio Chajnantor dome, Guacha caldera											
B06-024	53	lava	bio	22.6213	67.4668	301.0 ± 30.0	3.56 ± 0.16	1.60	3.59 ± 0.02	1.20	13 of 13
B06-024	53	lava	san	22.6213	67.4668	309.0 ± 16.0	3.50 ± 0.03	0.58	**3.51 ± 0.02**	0.63	22 of 22
Chajnantor lavas, Guacha caldera											
BOL-07-021	54	lava	san	22.6294	67.4136	295.7 ± 02.9	3.67 ± 0.10	1.5	**3.67 ± 0.13**	1.20	7 of 7
Rio Guacha dome, Guacha caldera											
B06-023	55	lava	bio	22.6107	67.4387	308.0 ± 12.0	3.57 ± 0.04	1.17	**3.61 + 0.02**	1.01	9 of 10
Alota dome, Alota ignimbrite shield											
92CJ018	56	lava	bio	21.4948	67.5831	298.3 ± 4.9	5.46 ± 0.06	1.18	5.49 ± 0.02	0.79	9 of 12
92CJ018	56	lava	san	21.4948	67.5831	290.9 ± 7.1	5.23 ± 0.04	1.00	**5.22 ± 0.02**	0.60	16 of 16

Note: Full analytical data in Appendix 2 (see text footnote 1). Preferred ages in bold.
*Map—refers to sample location numbers in Figure 6.
†Mat.—material from which minerals were extracted (pum—pumice; mat—matrix).
§Min.—mineral used in laser fusion analyses (bio—biotite; san—sanidine).
#MSWD—mean square of weighted deviations.
**Ages were calculated relative to 28.34 Taylor Creek sanidine (Renne et al., 1998); italicized biotite data are discordant and were not used in weighted mean calculations.
††Indicates sample with multiple crystal fusion analyses; all others analyzed by single-crystal laser fusions (SCLF).

TABLE 2. PREVIOUS UNIT AND AGE DESIGNATIONS OF CORRELATED ALTIPLANO-PUNA VOLCANIC COMPLEX IGNIMBRITES

Ignimbrite and correlated tuffs	K/Ar (Ma)	Age reference	Map*
Tatio ignimbrite			
Tatio Ig. (Chile)	0.71 ± 0.14†	Barquero-Molina (2003)	57
Tocopuri tuffs	1.3 ± 0.4	Choque et al. (1996)	58
Huayllajara tuffs			
Michina 1 tuffs			
Michina 2 tuffs			
Río Pabellon 2 tuffs			
Puripica Chico ignimbrite			
Puripica Chico tuffs			
Laguna Colorada ignimbrite			
Aguadita 4 tuffs	1.9 ± 0.2	Baker and Francis (1978)	4
	1.7 ± 0.5	Baker and Francis (1978)	59
Aguadita 3 tuffs			
Aguadita Brava tuffs§			
Pastos Grandes ignimbrite			
Pastos Grandes tuffs	3.2 ± 0.3	Lema and Ramos (1996)	60
	3.2 ± 0.4	Baker and Francis (1978)	61
	3.5 ± 0.3	Pacheco and Ramírez (1997a)	62
Chatola tuffs	3.2 ± 0.2	Baker and Francis (1978)	63
	3.6 ± 0.5	Pacheco and Ramírez (1997a)	64
Huayllar tuffs			
Tara ignimbrite			
Upper Tara (Chile)	3.42 ± 0.15	Lindsay et al. (2001a)	65
	3.77 ± 0.15	Lindsay et al. (2001a)	66
	3.65 ± 0.12	Lindsay et al. (2001a)	67
	3.82 ± 0.13	Lindsay et al. (2001a)	65
	3.81 ± 0.12	Lindsay et al. (2001a)	68
	3.83 ± 0.21	Lindsay et al. (2001a)	66
Aguadita Brava tuffs§			
Atana tuffs			
Chajnantor tuffs§			
Pampa Totoral tuffs			
Pampas Guayaques 1 tuffs§			
Pampas Guayaques 2 tuffs§			
Alota ignimbrite			
Juvina tuffs			
Guacha ignimbrite			
Aguadita 2 tuffs	4.5 ± 0.5	Pacheco and Ramírez (1997b)	69
Lower Tara (Chile)	5.47 ± 0.33	Lindsay et al. (2001a)	70
	5.62 ± 0.98	Lindsay et al. (2001a)	66
	5.68 ± 0.14	Lindsay et al. (2001a)	71
Inca tuffs	5.6 ± 0.5	Almendras et al. (1996)	72
Pampa Guayaques 1 tuffs§	5.9 ± 0.4	Almendras et al. (1996)	73
Tullitayoj tuffs	5.8 ± 0.4	Pacheco and Ramírez (1997c)	24
	6.2 ± 0.4	Pacheco and Ramírez (1997b)	74
Aguadita 1 tuffs	6.2 ± 0.5	Almendras et al. (1996)	75
	6.3 ± 0.4	Pacheco and Ramírez (1997b)	69
Quetena tuffs	6.5 ± 0.4	Pacheco and Ramírez (1997b)	76
Chajnantor tuffs§	6.6 ± 0.5	Almendras et al. (1996)	77
Kalina tuffs	6.6 ± 0.4	Almendras et al. (1996)	78
Delgada tuffs	6.9 ± 0.7	Choque et al. (1996)	79
Pampa Guayaques 2 tuffs§			
Chuhuilla ignimbrite			
Chuhuilla ignimbrite	5.9 ± 0.3	Baker and Francis (1978)	80
Tomasamil tuffs	6.0 ± 0.5	Almendras and Baldellón (1997)	22
	6.2 ± 0.7	Almendras and Baldellón (1997)	81
	6.3 ± 0.8	Pacheco and Ramírez (1997a)	82
	6.7 ± 0.6	Almendras and Baldellón (1997)	83
Thiumayu tuffs	7.4 ± 0.8	Pacheco and Ramírez (1997a)	84

Note: Ignimbrite units of this study underlined; correlated units are in plain text. Geologic map references with correlated tuffs not listed above: Fernández et al. (1996), García (1996), Pacheco and Ramirez (1996).

*Map refers to locations in Figure 6.

†$^{40}Ar/^{39}Ar$ age.

§Denotes units with outcrops that have been correlated with more than one ignimbrite unit in this study.

This behavior has also been observed in other Pliocene–Pleistocene silicic lavas and ignimbrites within the Central Andes and may reflect pre-eruption partitioning of a small quantity of excess argon into biotite that is retained upon eruption owing to the higher closure temperature of biotite relative to sanidine (Hora et al., 2010). Thus, the biotite dates likely yield maximum ages for those units.

K-Ar versus $^{40}Ar/^{39}Ar$ Ages

We determined $^{40}Ar/^{39}Ar$ ages for 13 ignimbrite samples from northern Chile that had previously been analyzed by the K-Ar method (de Silva, 1989b). K-Ar and $^{40}Ar/^{39}Ar$ ages are concordant for 11 of 13 samples, whereas, in two others, the $^{40}Ar/^{39}Ar$ age is older than the corresponding K-Ar age (Table 3; Fig. 4). Moreover, in each case, the 2σ analytical uncertainty of the $^{40}Ar/^{39}Ar$ age is smaller by a factor of 4–5 compared to the K-Ar ages. A significant implication of the new $^{40}Ar/^{39}Ar$ ages is that it is now possible to distinguish among ignimbrite units that had previously yielded concordant K-Ar ages.

Paleomagnetism and Whole-Rock Geochemistry

Characteristic remanent magnetism (ChRM) directions were determined for 45 sites in 10 ignimbrites. The ChRM data were especially useful in distinguishing ignimbrites in the central region of the study area where many of the large ignimbrite sheets overlap and will be the subject of a later publication. The results of 21 whole-rock geochemical analyses (19 unaltered blocks of pumice and 2 effusive post-ignimbrite lavas) are shown in Figure 5 and reported in full in Appendix 3 in the GSA Data Repository (see footnote 1). Analyses of samples with concordant $^{40}Ar/^{39}Ar$ ages are commonly consistent with respect to most major and trace elements and support correlations based primarily on the age determinations and field relations. The ignimbrites and lavas analyzed in this study are similar to previous measurements of Altiplano-Puna volcanic complex ignimbrites, i.e., dominantly high-K, calc-alkaline dacites with much lesser volumes of rhyodacites and rhyolites.

Unit Correlations and Preferred Ages

Most ignimbrite outcrops in the Lípez region are similar to Altiplano-Puna volcanic complex ignimbrites in Chile (de Silva, 1989b; de Silva and Francis, 1989; Lindsay et al., 2001a, 2001b; Schmitt et al., 2001) and Argentina (Soler et al.,

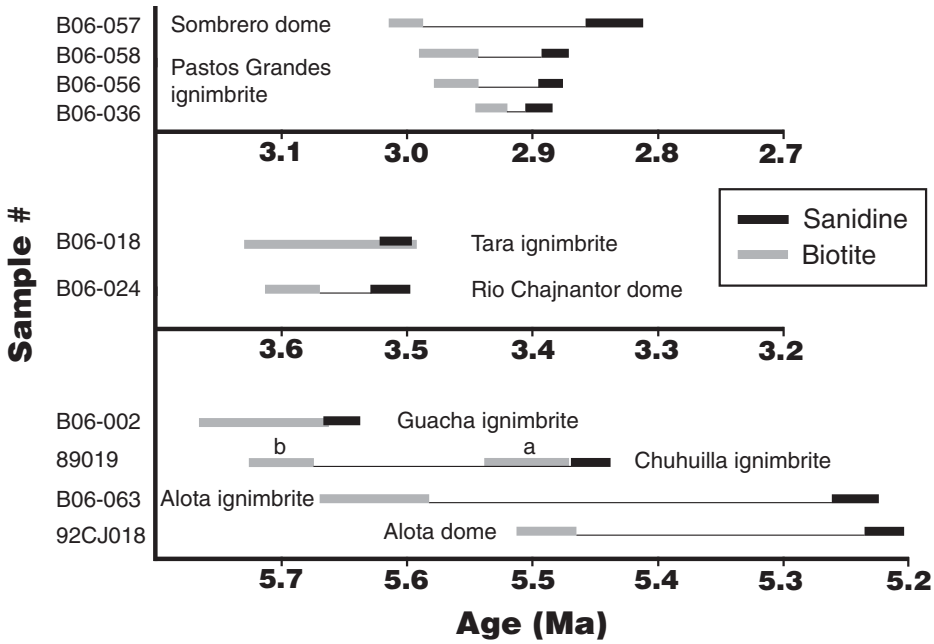

Figure 2. Comparison of $^{40}Ar/^{39}Ar$ results from coeval sanidine and biotite from common samples. Tie lines connect apparent ages for each sample. The bar width represents 2σ analytical uncertainty. The weighted mean ages of each mineral phase are only concordant in two samples (B06-018 and B02-002) for which the biotite has a large uncertainty. In other cases, sanidine ages are significantly younger.

2007); they are commonly buff in color and contain large (commonly up to 5 mm) phenocrysts of plagioclase, quartz, and biotite. Due to significant overlap in both whole-rock and mineral chemistry among the ignimbrite units, we relied heavily on field observations and high-precision $^{40}Ar/^{39}Ar$ age determinations supported by ChRM data to establish unit correlations as well as the eruption age for each ignimbrite. Positive correlations were made where all applicable samples within a unit yielded: (1) $^{40}Ar/^{39}Ar$ ages with Gaussian probability distributions and mean square weighted deviate (MSWD) values <1.5, (2) consistent paleomagnetic and stratigraphic field observations, and (3) comparable bulk chemical and mineralogical composition. Once correlation was established among sample sites, we used the age, geochemical, paleomagnetic, and previously published K-Ar ages to correlate the numerous outcrop distributions from the SERGEOMIN geologic maps of southwest Bolivia (Table 2; Fig. 6).

Ignimbrite Extent and Volumes

The sheer scale of these large ignimbrites and their source calderas, coupled with the vagaries of distribution, exposure, and preservation, particularly in older eruptions, makes volume estimation a nontrivial task. Examination of the literature (e.g., Mason et al., 2004) shows that, in many cases, volume estimations are often order of magnitude estimates that are loosely based on two rules of thumb: (1) that magma equivalent intracaldera and outflow deposit volumes are approximately equal and (2) that some outflow deposit volumes are approximately equal to coignimbrite ash volumes. Based on our experience in the Altiplano-Puna volcanic complex and at Cerro Galán, we find these rules untenable. First, intracaldera:outflow ratios range considerably based on collapse-style and timing. At La Pacana (Lindsay et al., 2001a), Vilama (Soler et al., 2007), and Cerro Galán (Folkes et al., 2010) intracaldera:outflow ratios are as high as 4:1 or 5:1.

Second, the crystal-rich nature of the monotonous intermediate magmas and minimal crystal enrichment in the bulk matrix compared to pumice suggest that fallout and ash volumes may not be as important as generally assumed. To date, no correlation of distal ash deposits of any significant volume has been realized for the Altiplano-Puna volcanic complex. So, the assumption of an equivalent outflow:ash-fall ratio is not supported in this work. To avoid these potential sources of overinflation of eruption volumes, we adopt a very conservative approach as described below.

Intracaldera Deposit Volume

Intracaldera volume is calculated based on excellent exposure of resurgent blocks of the Pastos Grandes and Guacha calderas, which reveal 1.3 and 1.1 km, respectively, of maximum relief between the resurgent intracaldera domes and their surrounding moats. These thicknesses consist of welded tuff and thus represent a minimum thickness of intracaldera ignimbrite. While the intracaldera deposits of the older eruptions from these nested caldera complexes are largely obscured, and the depth of collapse for these eruptions is unconstrained, we use a 1 km intracaldera thickness for the older eruptive units (Chuhuilla and Guacha ignimbrites). Similar thicknesses of at least 1.1 km are also seen in the other major caldera complex in this region (Lindsay et al., 2001a; Soler et al., 2007; Folkes et al., 2010). Unlike at La Pacana and Vilama calderas, where asymmetric caldera collapse was assumed and intracaldera thicknesses were extrapolated in volume calculations (Lindsay et al., 2001a; Soler et al., 2007), we do not make any similar adjustments to the intracaldera volumes of the Guacha, Chuhuilla, Tara, or Pastos Grandes ignimbrites.

For the ignimbrite shields (Laguna Colorada, Tatio, and Alota), we assume modest sag-type calderas (<65 km^2) with minimal intracaldera fill depths of 0.2 km. These estimates are based on the relatively large size of outflow sheets and evidence for the presence of a sag caldera beneath the effusive lavas of the Panizos ignimbrite shield (Ort, 1993). Intracaldera deposits have measured densities near dense rock equivalent (2.4 g/cm^3), and no adjustment is made to the deposit volumes.

Outflow Deposit Volumes

Although the relative youth and long-term aridity of the Altiplano-Puna volcanic complex result in mostly intact deposits, limited downcutting prevents accurate thickness estimates throughout the distribution of each ignimbrite. The available exposure, uplift local to the calderas, and distal mesas and other remnants, however, do allow useful thickness estimates for each unit to be determined from source to edge. While locally the outflow ignimbrites may be hundreds of meters thick (proximal to caldera, or valley ponded), typically the ignimbrites range from ~80 to 20 m throughout most of their extent, thinning distally to 10 m or less. We thus use an average of 50 m for the outflow deposit thickness, which is then multiplied by the areal extent of each unit to calculate the outflow volumes.

The areal extents of the deposits used for volume calculations are defined by the most distal outcrops we were able to correlate. Rather

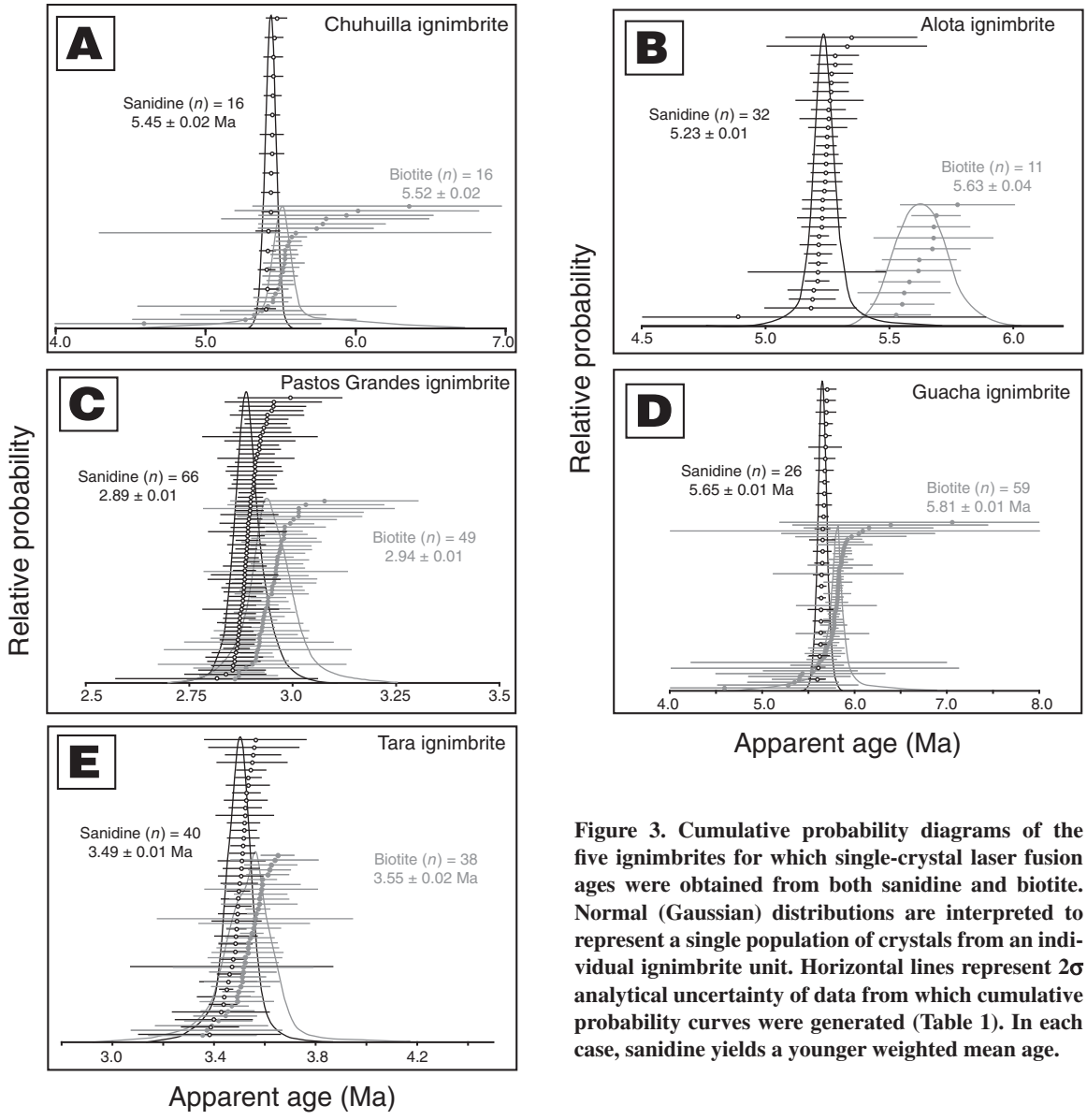

Figure 3. Cumulative probability diagrams of the five ignimbrites for which single-crystal laser fusion ages were obtained from both sanidine and biotite. Normal (Gaussian) distributions are interpreted to represent a single population of crystals from an individual ignimbrite unit. Horizontal lines represent 2σ analytical uncertainty of data from which cumulative probability curves were generated (Table 1). In each case, sanidine yields a younger weighted mean age.

than assume radial distribution, we attempted to generate shape files in the GIS that reflect the mapped distribution of the units, taking into account preexisting topography to the best extent of our knowledge. Older deposits are the most prone to error in this treatment. Based on measured bulk ignimbrite densities of 1.8–2.2 g/cm^3, DRE volumes are calculated to 75% of deposit volume.

While the long-term aridity of the plateau going back at least until 10 Ma has been well established (e.g., Strecker et al., 2007), local fluvial erosion has been persistent plateauwide. In the Altiplano-Puna volcanic complex, interplay between fluvial and eolian erosion is strongly documented in the ignimbrites (Bailey et al., 2007; de Silva et al., 2010), and there is clear

TABLE 3. NEW BIOTITE $^{40}Ar/^{39}Ar$ AGES VERSUS BIOTITE K-Ar AGES OF DE SILVA (1989b)

Sample no.	Lat (°S)	Long (°W)	$^{40}Ar/^{39}Ar$ (Ma, ±2σ)	K-Ar (Ma, ±2σ)	Ignimbrite
83078	23.59	67.88	2.51 ± 0.08	2.34 ± 0.22	Talabre
83077	23.18	67.98	3.96 ± 0.08	4.18 ± 0.28	Atana
83034	22.77	68.02	4.00 ± 0.10	4.29 ± 0.14	Chaxas
83015	22.70	68.24	4.05 ± 0.11	4.02 ± 0.22	Puripicar
83016	22.70	68.24	5.82 ± 0.08	5.71 ± 0.73	Pelon
83065	22.25	68.14	6.33 ± 0.12	5.65 ± 0.34	Linzor
83001	22.66	68.47	8.23 ± 0.15	8.29 ± 0.25	Sifon
83022B	22.66	68.23	8.30 ± 0.04	8.48 ± 0.56	Yerbas Buenas
83005	22.75	68.44	8.34 ± 0.07	7.76 ± 0.57	Sifon
83028	22.72	68.22	9.35 ± 0.03	9.39 ± 0.28	Artola
83002	22.66	68.47	9.45 ± 0.03	9.53 ± 0.36	Artola
83050	22.28	68.29	10.18 ± 0.15	10.60 ± 0.62	Divisoco
83088	22.02	68.62	10.71 ± 0.14	9.66 ± 0.49	Lower Rio San Pedro

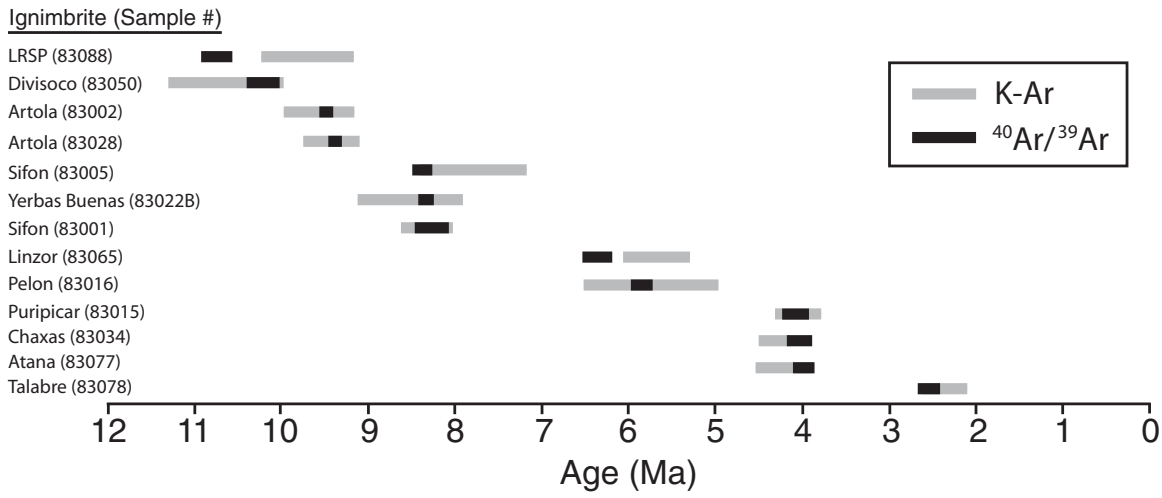

Figure 4. Comparison of $^{40}Ar/^{39}Ar$ results from this study with K-Ar results from the same samples reported in de Silva (1989b). The length of each line represents the 2σ analytical uncertainties. In 8 of the 11 samples, the $^{40}Ar/^{39}Ar$ ages are concordant, and all are more precise than the corresponding K-Ar age.

evidence that distal ignimbrite deposits have been completely removed. However, this loss is local and windward and certainly not pervasive throughout the extent of the ignimbrites. Moreover, the amount removed by erosion is a function of material properties of ignimbrite leach (induration, welding, etc.; de Silva et al., 2010). We do not attempt to estimate the amount of material removed by erosion.

Volumes of Fallout and Coignimbrite Ash

Similarly, we make no consideration for loss of fallout or coignimbrite ash. The lack of regionally extensive Plinian fall precursors to these large-volume ignimbrites is documented in many areas beyond the Central Andes, and this may suggest low-fountaining eruption columns that do not generate significant Plinian fallout (e.g., de Silva et al., 2006b). Ort (1993) has argued that the extremely crystal-rich nature of the Panizos ignimbrites (50% crystals in the pumice), which are similar to many other Altiplano-Puna volcanic complex ignimbrites, resulted in ash-poor ignimbrites that would only be weakly fluidized and that elutriation of fine ash would be inefficient. Preliminary estimates of crystal enrichment in the Cerro Galán ignimbrites (Folkes et al., 2010) and the Puripicar and Atana ignimbrites of northern Chile suggest crystal enrichment of only 10%–15%, i.e., much lower than would be expected if approximately equivalent volumes of outflow and fallout ash (co-plinian or coignimbrite) were erupted.

As outlined already, our approach minimizes potential errors and yields minimum ignimbrite volumes (Table 4). The largest error in our estimates is in the lack of constraint on topographic control of the older ignimbrites beneath the Vilama in Bolivia and the Sifon in Chile. However, sufficient incision and basement exposure indicate that these are rather confined and not as laterally extensive as the younger ignimbrites (e.g., de Silva, 1989b; Caffe et al., 2008). Further detailed mapping may refine our figures if new exposures are found, with the most significant changes likely to come when the Guacha and Pastos Grandes calderas are mapped and studied in more detail, which we suspect will only increase our volume estimates.

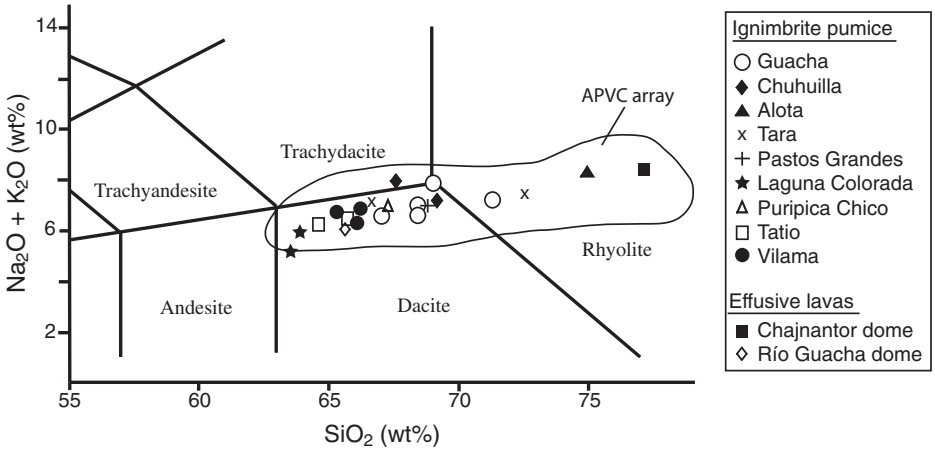

Figure 5. Total alkalis versus silica diagram of pumice from Bolivian ignimbrites and lavas analyzed in this study. Also shown is array of Altiplano-Puna volcanic complex (APVC) ignimbrite pumice reported in de Silva (1987), Lindsay et al. (2001b), Ort et al. (1996), and Soler et al. (2007). Altiplano-Puna volcanic complex ignimbrites and lavas are dominantly dacitic with lesser volumes of rhyolite.

CORRELATION, DISTRIBUTIONS, AND VOLUMES OF LIPEZ IGNIMBRITE UNITS

Pastos Grandes Caldera Complex

Chuhuilla Ignimbrite

The Chuhuilla ignimbrite is the northernmost large-volume ignimbrite of the Altiplano-Puna volcanic complex and was linked with the Pastos Grandes caldera complex when the ~60 × 35 km, oval collapse structure was first identified through satellite imagery (Baker, 1981). Chuhuilla pumice is crystal-rich,

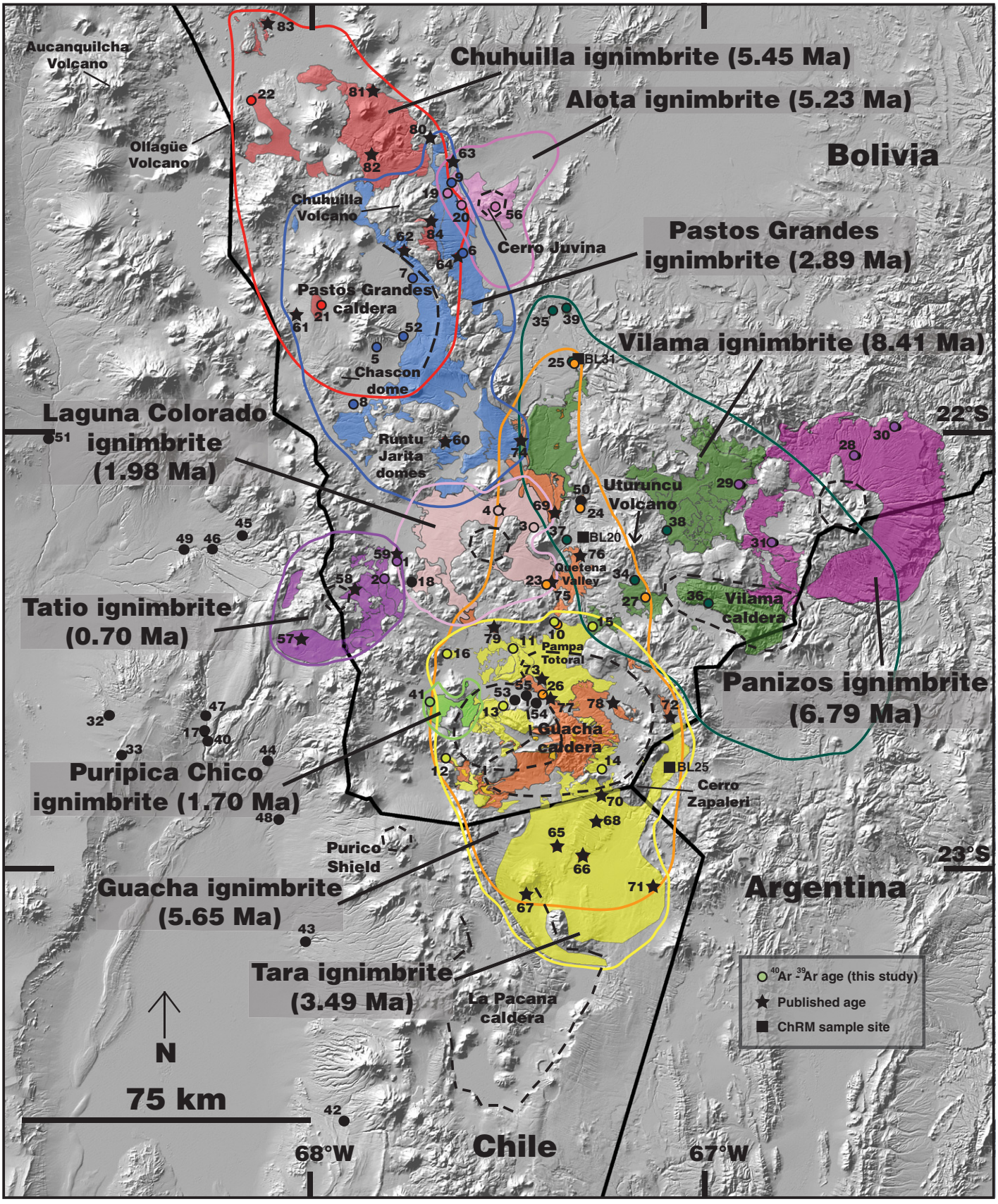

Figure 6.

Figure 6. Location map showing sample localities and estimated original ignimbrite distributions (thick colored outlines) of newly described ignimbrite units from the Bolivian Altiplano-Puna volcanic complex. Extents of previously described Vilama (Soler et al., 2007) and Panizos (Ort, 1993) ignimbrites are also shown, with minor modification to the Vilama as described in the text. Outcrops from the SERGEOMIN geologic maps (filled polygons) are color-coded to demonstrate correlations to each ignimbrite unit (see Table 3 for references and original outcrop names). Distributions of Tara and Guacha ignimbrites in Chile are from Lindsay et al. (2001a). $^{40}Ar/^{39}Ar$ sample locations from this study are shown as circles; stars are published isotopic age data used to aid in correlating ignimbrites in this study (see Table 2 for references). Map numbers correspond with $^{40}Ar/^{39}Ar$ and K-Ar dates listed in Tables 1 and 2 (previously published age data for Vilama and Panizos ignimbrites are not shown). Dashed lines show approximate or inferred locations of caldera collapse scarps. Locations of characteristic remanent magnetism (ChRM) sample sites discussed in Appendix 1 (see text footnote 1) are shown as squares. Base map is a digital elevation model (DEM) made from 90 m Shuttle Radar Topography Mission (SRTM) data.

containing large, purple phenocrysts of quartz commonly >5 mm, and large euhedral biotite. Within the pumice, dense, crystal-rich enclaves of euhedral plagioclase, quartz, biotite, and amphibole are common. No fallout was identified for this unit. Two analyzed pumice blocks contain 68–69 wt% SiO_2.

Baker and Francis (1978) determined a biotite K-Ar age of 5.9 ± 0.3 Ma for the Chuhuilla ignimbrite, whereas our $^{40}Ar/^{39}Ar$ age determinations for two biotite samples yielded discordant results. Biotite from sample B06-050 gave a $^{40}Ar/^{39}Ar$ date of 5.54 ± 0.03 Ma, whereas the age distribution from biotite from sample 89019 was bimodal (Fig. 2), with four of the ages concordant with sample B06-050 (Table 1). Sanidine from sample 89019 gave a normal probability distribution (Fig. 3A) and our preferred age of 5.45 ± 0.02 Ma.

The Chuhuilla ignimbrite crops out primarily to the north of Pastos Grandes caldera and in valley exposures between Cerro Juvina and the caldera. Sample 89019, however, was collected west of the Pastos Grandes resurgent dome and supports a larger distribution for this unit. We correlated the distribution of the Chuhuilla ignimbrite of Baker (1977, 1981) with the Tomasamil and Thiumayu tuffs of the geologic maps (Almendras and Baldellón, 1997; Pacheco and Ramírez, 1997a) based on outcrop distributions and similar K-Ar ages (Table 2). The ignimbrite unit likely extends farther west and north than the mapped extent, but is buried beneath the modern arc deposits. On the Chilean side of the border, the 5.4 ± 0.3 Ma (K-Ar age of Baker and Francis, 1978) rhyolitic Carcote ignimbrite is stratigraphically equivalent but compositionally distinct from the dacitic Chuhuilla ignimbrite, and we therefore consider them separate units, although they have not been found in contact in the field. Southward into Chile, the Toconce and Linzor tuffs are also stratigraphically and chronologically equivalent to the Chuhuilla ignimbrite, but the source of these small-volume ignimbrites is in northern Chile (de Silva, 1989b). Our current map of the distribution of the Chuhuilla ignimbrite covers an area of ~4000 km^2 (Fig. 6). Increases in thickness and welding toward the Pastos Grandes caldera support the Baker and Francis (1978) suggestion that the source of the Chuhuilla ignimbrite is in the area of the current Pastos Grandes caldera. It remains to be determined if the large Pastos Grandes collapse scarp is related to the Pastos Grandes ignimbrite (described later herein) or whether this is a Chuhuilla-aged structure that was reactivated during the younger eruption. Lavas from the Chuhuilla stratovolcano define the crest of the scarp, lie stratigraphically above the Chuhuilla ignimbrite, and may represent postignimbrite eruptions along the ring fracture. We note that the K-Ar date of 7.3 ± 0.5 Ma for the Chuhuilla lavas (Pacheco and Ramírez, 1997a) is inconsistent with the stratigraphy because they overlie the 5.45 Ma Chuhuilla ignimbrite. Assuming the Pastos Grandes collapse scarp is indeed related to the Chuhuilla caldera, we calculate an intracaldera area of ~1100 km^2, an outflow area of ~3170 km^2, and a minimum DRE volume of ~1200 km^3 for the Chuhuilla ignimbrite (Fig. 6; Table 4).

Alota Ignimbrite

The rhyolitic Alota ignimbrite shield (also known as Cerro Juvina) is located ~10 km east of the Chuhuilla stratovolcano within the broad Alota basin. It consists of a gently sloping (~4%–6%) ignimbrite apron with lava flows stratigraphically above the center of the shield. Downcutting around the domes reveals the contact between the lavas and the pyroclastic units to be conformable and consistent with postignimbrite effusive activity above the pyroclastic base. Pumice from the Alota ignimbrite is among the most silicic (75 wt% SiO_2) measured within the Altiplano-Puna volcanic complex.

Prior to this study, the only age for this center was a 6.5 ± 0.3 Ma K-Ar determination from biotite in the central lava complex (Pacheco and Ramírez, 1997a). Sanidine from dome lava yields a $^{40}Ar/^{39}Ar$ age of 5.22 ± 0.01 Ma, which is indistinguishable from the Alota ignimbrite pumice age of 5.23 ± 0.01 Ma (Table 1).

The Alota ignimbrite is largely restricted to the Alota basin, suggesting that the currently exposed sedimentary sequences to the east, and

TABLE 4. VOLUME CALCULATIONS FOR NEWLY DESCRIBED IGNIMBRITES

	Intracaldera*			Outflow†			
Ignimbrite	Area (km^2)	Thickness (km)	Volume (km^3)	Area (km^2)	Thickness (km)	Volume (km^3)	Total DRE§ (km^3)
Pastos Grandes	1100	1.3	1430	2900	0.05	145	1500
Guacha	1150	1.0	1150	4650	0.05	233	1300
Chuhuilla	1100	1.0	1100	3170	0.05	159	1200
Tara	620	1.1	682	3480	0.05	174	800
Laguna Colorada	63	0.2	12.6	1100	0.05	56	60
Tatio	54	0.2	10.8	830	0.05	42	40
Alota	15	0.2	3	520	0.05	26	20
Puripica Chico				150	0.05	8	10

*Thickness of intracaldera deposit estimated as maximum relief between resurgent dome and caldera moat.
†Area of outflow does not include intracaldera area.
§Total dense rock equivalent (DRE) = (0.75 × [outflow volume] + [intracaldera volume]) and rounded to nearest 10 or 100 km^3; 0.75 factor based on average densities of ~1.8 g/cm^3 calculated for outflow bulk matrix of Altiplano-Puna volcanic complex ignimbrites.

the Chuhuilla stratovolcano to the west acted as topographic barriers. Our estimate of the Alota ignimbrite outflow distribution (Fig. 6) includes a modest extension of the Juvina tuffs of Pacheco and Ramírez (1997a). Incision around the effusive dome lavas reveals evidence of proximal thickening of the pyroclastic sequence. This suggests a shallow sag structure in which the proximal deposits are assumed to have ponded. An overall volume of at least ~20 km^3 DRE is calculated for this ignimbrite.

Pastos Grandes Ignimbrite

In the Alota basin, three major ignimbrite units are clearly exposed with the 5.45 Ma Chuhuilla ignimbrite overlain by the 5.23 Ma Alota ignimbrite, and the 2.89 Ma Pastos Grandes (Fig. 7A). Pumice in the Pastos Grandes ignimbrite is rare and, where present, is strongly indurated and difficult to extract. No fall deposit is associated with this thick, homogeneous ignimbrite unit.

The eastern outflow of the Pastos Grandes ignimbrite was mapped by Pacheco and Ramírez (1997a) as the Chatola tuffs, with two K-Ar ages between 3 and 4 Ma (Baker and Francis, 1978; Pacheco and Ramírez, 1997a). This outflow unit, just east of the Pastos Grandes caldera scarp, is thick and highly indurated, consistent with a relatively proximal source. Pacheco and Ramírez (1997a) argued that eruption of the outflow Chatola tuffs was responsible for the collapse of the Pastos Grandes caldera, which was then closely followed by eruption of the intracaldera Pastos Grandes tuffs. However, based on the concordant ages of the intracaldera and outflow units, and the thick (1.3 km) resurgent mound of intracaldera ignimbrite, we argue that caldera collapse likely occurred early in the eruption and emplaced a single unit, the Pastos Grandes ignimbrite. We have also correlated outcrops to the south of the caldera with the Pastos Grandes ignimbrite based on flow distribution patterns and ChRM signatures.

Figure 7. (A) View looking south from drainage of Río Chaira Waykho between the Pastos Grandes caldera and the Alota ignimbrite shield. ~100 m of total exposed ignimbrite shown in image. (B) View looking northeast from rim of Pampa Totoral towards the Quetena Valley and Uturuncu volcano. Erosion along the Quetena River has exposed the confluence of the 5.65 Ma Guacha ignimbrite and the 1.98 Ma Laguna Colorada ignimbrite. The 8.41 Vilama ignimbrite is exposed in limited outcrops below the Guacha ignimbrite within the canyon in the northern valley. Distance from road (elevation 4300 m) in bottom right of image to the summit of Uturuncu volcano (elevation 6008 m) is ~25 km.

Abundant sanidine from both intracaldera and outflow samples, combined with sanidine from the resurgent dome, yielded a precise weighted mean age of 2.89 ± 0.01 Ma, which is our preferred eruption age for the Pastos Grandes ignimbrite. Biotite produced a slightly older weighted mean age of 2.94 ± 0.01 Ma (Fig. 3C). The previously undated Pastos Grandes resurgent ignimbrite dome yielded a biotite ^{40}Ar/^{39}Ar age of 2.91 ± 0.03 Ma, which strongly suggests that the resurgent dome is composed of the Pastos Grandes ignimbrite, although we were unable to find sanidine in this sample, which is common in other Pastos Grandes samples. A stratigraphically consistent sanidine ^{40}Ar/^{39}Ar age of 2.83 ± 0.02 Ma for the Cerro Sombrero lava dome (Table 1; Fig. 6) overlying the eastern edge of the resurgent dome supports the argument that effusive activity and resurgence closely followed eruption of the Pastos Grandes ignimbrite.

As mentioned above, it is less obvious whether the giant Pastos Grandes caldera scarp also formed during this eruption, or is a remnant of the Chuhuilla ignimbrite eruption and associated collapse. Both ignimbrites are widespread, and large collapse structures would be expected from both eruptions. As a first-order approximation, we assume the same area for intracaldera Pastos Grandes as for the intracaldera Chuhuilla ignimbrite, although further investigation is necessary to clarify the collapse structure(s). From our estimates, we calculate a minimum intracaldera volume of 1430 km^3 based on the exposed thickness of the resurgent domes, an outflow distribution of at least 2900 km^2 (Fig. 6), and a total minimum volume of 1500 km^3 DRE (Table 4).

Guacha Caldera Complex

Guacha Ignimbrite

During study of the La Pacana caldera in northern Chile, Lindsay et al. (2001a) identified two new extensive ignimbrite units that had previously been attributed to the Atana ignimbrite by Gardeweg and Ramírez (1987). Lindsay et al. (2001a) named these units the Lower and Upper Tara ignimbrites and argued for a Bolivian source near Cerro Guacha or Cerro Corutu. We have mapped both of these ignimbrites into Bolivia, which we here rename the Guacha and Tara ignimbrites, respectively. The Guacha ignimbrite is a crystal-rich rhyodacite (67–71 SiO_2 wt%) with a wide distribution in Bolivia, Chile, and Argentina. Lindsay et al. (2001a) determined three biotite K-Ar ages between 5.5 and 5.7 Ma for this ignimbrite in Chile. In contrast, 59 new single-crystal fusion biotite ^{40}Ar/^{39}Ar ages from five suspected Guacha samples gave

a weighted mean age of 5.81 ± 0.01 Ma. In only the northernmost of these samples were we able to locate and analyze sanidine, which yielded the younger, preferred, age of 5.65 ± 0.01 Ma. This northern sample, collected just above the Vilama ignimbrite, is located more than 130 km from an outcrop of the Guacha ignimbrite (formerly Lower Tara) identified by Lindsay et al. (2001a) on the shores of the Salar de Tara in Chile, thus identifying the Guacha ignimbrite as among the most widespread within the Altiplano-Puna volcanic complex. This interpretation is supported by evidence for a large caldera collapse of Cerro Guacha associated with the eruption, including a wide distribution of welded, apparently intracaldera ignimbrite as well as a large, westward-concave, arcuate scarp partially obscured by effusive lavas east of the resurgent ignimbrite. An outcrop of welded ignimbrite with subvertical lineation and abundant lithics was found just west of the scarp and is likely one of the vent locations for the Guacha ignimbrite. Densely welded intracaldera outcrops ~30 km from the scarp are consistent with a large (~1200 km^2) trapdoor collapse area with dimensions among the largest recorded (Mason et al., 2004). Mapping from La Pacana caldera northward has identified the Guacha ignimbrite as forming the southern flank of the Guacha caldera and forming the eastern portion of the resurgent dome, while the western dome is unequivocally related to the Tara ignimbrite (Fig. 6), as described in the next section. The inner eastern collapse scarp of the Guacha caldera (formed during the younger Tara ignimbrite eruption) reveals a >700-m-thick section of eastward-dipping Guacha ignimbrite suggesting truncation of the Guacha resurgent dome by collapse associated with the later eruption.

The outflow of the Guacha ignimbrite crops out beneath the Tara ignimbrite and extends into the Quetena Valley (Fig. 7B) between the Laguna Colorada ignimbrite shield and Uturuncu volcano and continues northward for at least another 60 km. The Guacha ignimbrite is also found to the east and south of Uturuncu volcano, and its apparent north-south trend suggests that the outflow followed a broad paleovalley, now occupied by the Quetena River.

Younger deposits largely obscure the western extent of this ignimbrite. A discordantly younger (compared to other biotite and sanidine dates from this unit) biotite $^{40}Ar/^{39}Ar$ age of 5.52 ± 0.06 Ma was determined from pumice (B06-085) sampled at the southern end of the Quetena Valley. Based on continuity of the ignimbrite sheet to the south and north of this location, however, we attribute this age discordance to loss of radiogenic argon from biotite in sample B06-085.

Numerous outcrops dated with the K-Ar method between 5 and 8 Ma and reported on the geologic maps as nine separate units are correlated with the Guacha ignimbrite (Table 2) based on field relations. In total, the Guacha ignimbrite covers a region of at least 5800 km^2, including the portions mapped in Chile by Lindsay et al. (2001a). Combined intracaldera and outflow volume estimates yield an overall minimum volume of 1300 km^3 DRE (Table 4). The actual volume is likely much higher based on observed thicknesses and the large size of the caldera structure.

Tara Ignimbrite

Lindsay et al. (2001a) determined six K-Ar ages ranging from 3.42 ± 0.15 to 3.83 ± 0.21 Ma for Tara ignimbrite (formerly Upper Tara) outcrops in northeastern Chile. As one of the best-exposed units in the Altiplano-Puna volcanic complex, we have mapped this ignimbrite between Bolivia, Chile, and Argentina (Fig. 6). The thickest deposits are found in the ~1-km-thick western resurgent dome within the Guacha caldera, and outflow outcrops extend predominantly to the north and southeast of the resurgent dome. Contacts between the Guacha ignimbrite and the Tara ignimbrite are common. Outside the Guacha caldera, >200-m-thick accumulations of the Tara underlie Cerro Zapaleri near the triple point of the borders of Bolivia, Chile, and Argentina.

A sample from the western end of the resurgent ignimbrite dome yielded a $^{40}Ar/^{39}Ar$ biotite age of 3.56 ± 0.02 Ma, which is younger than the age inferred on the geologic maps. This age, combined with those of three outflow samples to the west, east, and north of the resurgent dome, gives a near-normal probability distribution curve (Fig. 3E) and a $^{40}Ar/^{39}Ar$ biotite age of 3.55 ± 0.02 for the Tara ignimbrite. We traced this ignimbrite north of the resurgent dome along the Pampa Totoral up to the southern end of the Quetena Valley, where the ignimbrite apparently stopped or has been completely eroded away. Two pumice samples from the Pampa Totoral yielded slightly older $^{40}Ar/^{39}Ar$ biotite ages (ca. 3.87 Ma). A single pumice analysis from the younger group revealed a rhyolitic composition, whereas pumice from the older group was dacitic. Our preferred age for the Tara ignimbrite comes from the only two samples of suspected Tara in which we were able to identify and analyze sanidine, which gave a weighted mean age of 3.49 ± 0.01 Ma. Three lava domes stratigraphically overlie the northern side of the resurgent ignimbrite dome, two of which were dated and yielded $^{40}Ar/^{39}Ar$ ages concordant or slightly older than the Tara ignimbrite, suggesting that effusive activity closely followed the ignimbrite-producing eruption. Whole-rock analyses of the two dated domes show strikingly different chemistry (Fig. 5) and mineralogy. The western, sanidine-bearing Chajnantor dome is among the most silica-rich (77 wt% SiO_2) samples analyzed in this study, whereas the middle, Río Guacha dome is dacitic (66 wt% SiO_2) and contains amphibole and rare pyroxene. Lindsay et al. (2001a) determined a rhyolitic composition for the Upper Tara ignimbrite with analyses that fall between the two domes in both major- and trace-element compositions. Least-squares mass-balance modeling of lava and pumice compositions precludes a simple crystal fractionation model to explain the chemical variability, and the wide range in composition and mineralogy is suggestive of a complex magmatic system.

Our mapping of the Tara ignimbrite in Bolivia contrasts with the SERGEOMIN geologic maps, which do not include an ignimbrite of a similar age. Field mapping of the Tara ignimbrite led us to correlate two undated units from the geologic maps and to also incorporate select outcrops that were previously correlated with older eruptions (Table 2). Overall, the Tara ignimbrite covers at least 2300 km^2 in Bolivia, in addition to the 1800 km^2 mapped in Chile by Lindsay et al. (2001a) and a lesser area in Argentina. A minimum volume of 800 km^3 DRE is estimated for the Tara ignimbrite (Table 4).

Puripica Chico Ignimbrite

During our investigations of the Guacha caldera complex, we sampled pumices from the small (~10 km^3) local ignimbrite that forms the hoodoos known to tourists as the Piedras de Dali, named for surreal spires of weathered, indurated ignimbrite. This pumice is dacitic (67.3 wt% SiO_2), and biotite yields a $^{40}Ar/^{39}Ar$ age of 1.72 ± 0.01 Ma, the youngest associated with the Guacha caldera. The source of this ignimbrite, named the Puripica Chico tuffs on the geologic maps (Choque et al., 1996; Fernández et al., 1996), appears to be buried under the Puripica Chico lavas, which erupted on the western edge of the Guacha collapse (Fig. 6). Structural and topographic evidence for collapse in this area is not found, but we note the similarity to the northern end of La Pacana caldera, where Lindsay et al. (2001a) identified the hinge of a trapdoor caldera. A similar collapse is posited for the Guacha caldera.

Vilama Caldera Complex

Vilama Ignimbrite

The extensive Vilama ignimbrite was described in detail by Soler et al. (2007), who used K/Ar and $^{40}Ar/^{39}Ar$ determinations to ascribe an

eruption age between 8.4 and 8.5 Ma and estimated a volume of 1000–1400 km^3 DRE. We sampled the Vilama ignimbrite throughout the eastern Lípez region and determined a weighted mean eruption age of 8.41 ± 0.02 Ma from 77 single-crystal biotite analyses from seven samples of both bulk matrix and pumice (Fig. 6; Table 1). Additionally, two Vilama outcrops were found along the Quetena River ~20 km further north than the distribution estimated by Soler et al. (2007). This modest extension is the only modification made to the distribution of Soler et al. (2007) shown in Figure 6.

Altiplano-Puna Volcanic Complex Ignimbrites without Association to Major Collapse Calderas

Laguna Colorada Ignimbrite

The dacitic Laguna Colorada ignimbrite shield, the focus of extensive explosive and effusive activity, lies between the Pastos Grandes and Guacha calderas. The ~40-km-diameter shield is referred to as the Panizos ignimbrite shield on the geologic maps (e.g., Pacheco and Ramírez, 1996) but is here referred to as the Laguna Colorada ignimbrite shield following de Silva and Francis (1991), who named it after the red-colored lake west of the shield and to distinguish this eruption from the better known and larger Panizos ignimbrite shield (Baker, 1981; Ort, 1993) in the eastern Altiplano-Puna volcanic complex. Previous K-Ar age determinations on biotite and hornblende yielded ages of 1.9 ± 0.2 Ma and 1.7 ± 0.5 Ma, respectively (Baker and Francis, 1978). The Laguna Colorada ignimbrite includes an ~2 m Plinian fall deposit at its base and at least two ~10-cm-thick locally intercalated fall deposits within the ignimbrite. It is overlain by extensive effusive lavas and lacks an obvious collapse structure. Observations here and at other centers of this type (Panizos, Purico, Alota) suggest the lavas may be constrained within a shallow sag structure on the ignimbrite platform (Baker, 1977; de Silva and Francis, 1991; Ort, 1993). Pumice from within the fall deposit and a highly indurated pumice from the top of the ignimbrite yielded the lowest SiO_2 values (63.6–63.9 wt%) of the Bolivian ignimbrites analyzed in this study.

The $^{40}Ar/^{39}Ar$ analyses of biotite from two samples of welded ignimbrite matrix from the northern and eastern edges of the ignimbrite apron gave a weighted mean age of 1.98 ± 0.03 Ma. The Laguna Colorada ignimbrite was previously described as the Aguadita 3 and Aguadita 4 tuffs, and we include select outcrops of the Aguadita Brava tuffs (Table 2) to establish an outflow areal extent of ~1100 km^2. Based on the distribution of the summit lavas, which are likely obscuring a central vent area and welded ignimbrite, we define a modest proximal deposit of ~63 km^2, and calculate a minimum total deposit volume of 60 km^3 DRE.

Tatio Ignimbrite

The Tatio ignimbrite (Lahsen, 1982) is preserved in outcrops south of Laguna Colorada and southwest of the Laguna Colorada ignimbrite shield. Similar to the Laguna Colorada ignimbrite, two of the dated samples of Tatio ignimbrite are less evolved (64.6–65.8 wt% SiO_2) than most of the larger Altiplano-Puna volcanic complex ignimbrites (Fig. 5). Biotite from three samples collected in this region yields a weighted mean age of 0.703 ± 0.010 Ma, which is concordant with the $^{40}Ar/^{39}Ar$ age for this ignimbrite reported in Barquero-Molina (2003) from Chile.

We correlated the Tatio ignimbrite with the Tocorpuri, Michina 1 and 2, and Río Pabellón 2 tuffs of the Bolivian geologic maps based on continuity in the field and a reported K-Ar age of 1.3 ± 0.4 Ma for the Tocorpuri tuffs (Table 2). Lahsen (1982) suggested the younger than 1 Ma Tocorpuri rhyolitic lava dome as a possible source area for the Tatio ignimbrite. Although we found no obvious source, deposit characteristics and facies distribution suggest that it is likely buried beneath younger deposits from Cerro del Tatio. We estimate an areal extent of ~830 km^2 and a total minimum volume of 40 km^3 DRE for this ignimbrite.

DISCUSSION

Spatial and Temporal Patterns of Altiplano-Puna Volcanic Complex Volcanism: Relation to Plate Kinematics and Implications for the Development of Large Silicic Magmatic Systems

The high-resolution geochronology, spatial distributions, and volume estimates presented in this study, in conjunction with previously published data, allow the realization of a comprehensive framework for the development of the Altiplano-Puna volcanic complex ignimbrite flare-up (Table 5; Fig. 8). The spatiotemporal evolution of the >12,800 km^3 of Altiplano-Puna volcanic complex ignimbrites during its ~11 m.y. duration (average 1.11 km^3/k.y.) is evaluated in 1.5 m.y. (and one 2.0 m.y) time slices in Table 6 and Figure 9. A cumulative volume-time relationship is shown in Figure 10. These data show that initial, small-volume, ignimbrite-producing volcanism was widespread throughout the complex represented by localized deposits now cropping out in Chile and Argentina (Fig. 9A). Major ignimbrite volcanism in the Altiplano-Puna volcanic complex began some 2 m.y. later with the eruption of the Vilama and Sifon ignimbrites at 8.41 and 8.33 Ma, respectively (Fig. 9B). These near-concordant eruptions mark the first peak (pulse 1; 30 km^3/yr) of intermediate, ignimbrite volcanism in the complex, and the distant areal distributions suggest that wide-scale construction of a Cordilleran-sized batholith had begun by this time (de Silva and Gosnold, 2007). The rates of ignimbrite volcanism apparently waned during the period between 7.5 and 6.0 Ma, although volcanism continued to be widespread across the region, as demonstrated by the eruption of the Panizos ignimbrite shield east of the Vilama caldera. Also erupting during this time frame, the Coranzulí ignimbrites (Seggiaro and Aniel, 1989; Seggiaro, 1994) in the southeast of the complex and minor ignimbrite volcanism occurred in the west (Fig. 9C). Volcanism increased in both volume and space between 6.0 and 4.5 Ma and is highlighted by the second major ignimbrite peak (pulse 2; 20 km^3/k.y.) between 5.60 and 5.45 Ma with the Guacha, Chuhuilla, and Pujsa ignimbrites erupting from the Guacha, Pastos Grandes, and La Pacana caldera complexes situated in a near north-south alignment behind the active arc front. This prodigious ignimbrite volcanism increased further between 4.5 and 3.0 Ma, a period characterized by the highest average eruption rates (2.08 km^3/k.y.) and the largest ignimbrite peak (pulse 3; 31 km^3/k.y.) with the eruption of the 4.09 Ma Puripicar and 3.96 Ma Atana ignimbrites occurring over a period of only ~100 k.y. During this highly productive interval, ignimbrite volcanism apparently became more focused near ~23°S. Pulse 3 was closely followed by two more VEI 8 eruptions, the 3.49 Ma Tara and 2.89 Ma Pastos Grandes ignimbrites. Including these two eruptions in the calculation of the third pulse (pulses 3a and 3b in Table 6), the eruption rate remains substantially higher (6.84–4.62 km^3/k.y.) than the average rate of 1.17 km^3/k.y., lasting up to 1 m.y. and marking this period as the climax of Altiplano-Puna complex volcanism. Following the eruption of the Pastos Grandes ignimbrite, the eruption rate decreases significantly to 0.10 km^3/k.y. during the final 1.5 m.y., when explosive eruptive activity was confined to the shield-building activity of the 0.98 Ma Purico (Schmitt et al., 2001) and 0.70 Ma Tatio ignimbrites, as well as minor eruptions such as the 0.53 Ma Tuyajto (Barquero-Molina, 2003) and <1 Ma Filo Delgado ignimbrites (Gardeweg and Ramírez, 1987). Eruption of these ignimbrites, along with silicic dome complexes with

TABLE 5. SUMMARY OF ALL MAJOR ALTIPLANO-PUNA VOLCANIC COMPLEX IGNIMBRITE PREFERRED AGES AND VOLUMES

Ignimbrite	Age (Ma, ±2σ)	Min.*	Volume† (km^3)	Caldera/shield source	Age reference
Filo Delgado	<1 Ma[§]	N.A.[#]	10[1]	La Pacana	Gardeweg and Ramírez (1987)
Tuyajto	0.53 ± 0.17	bio	N.D.**	N.D.	Barquero-Molina (2003)
Tatio	0.70 ± 0.01	bio	40	Tatio	This study
Purico	0.98 ± 0.03	bio	100[2]	Purico	Barquero-Molina (2003)
Puripica Chico	1.70 ± 0.02	bio	10	Guacha	This study
Laguna Colorada	1.98 ± 0.03	bio	60	Laguna Colorada	This study
Talabre	2.42 ± 0.06	plag	N.D.	N.D.	Barquero-Molina (2003)
Patao	2.52 ± 0.06	plag	N.D.	La Pacana	Barquero-Molina (2003)
Pastos Grandes	2.89 ± 0.01	san	1500	Pastos Grandes	This study
Tara	3.49 ± 0.01	san	800	Guacha	This study
Atana	3.96 ± 0.02	san	1600[3]	La Pacana	Barquero-Molina (2003)
Chaxas II	4.00 ± 0.10	bio	N.D.	N.D.	This study
Puripicar	4.09 ± 0.02	bio	1500[1]	N.D.	This study
Toconao	4.0–4.5[§]	N.A.	>100[3]	La Pacana	de Silva (1989b)
Alota	5.23 ± 0.01	san	20	Alota	This study
Carcote	5.4 ± 0.3[§§]	bio	n.d.	Unknown	Baker and Francis (1978)
Chuhuilla	5.45 ± 0.02	san	1200	Pastos Grandes	This study
Pujsa	5.6 ± 0.2[§§]	bio	>500[1]	La Pacana	de Silva (1989b)
Guacha	5.65 ± 0.01	san	1300	Guacha	This study
Pelon	5.82 ± 0.08	bio	>100[1]	N.D.	This study
Linzor	6.33 ± 0.12	bio	N.D.	N.D.	This study
Toconce	6.52 ± 0.19	bio	N.D.	N.D.	This study
Coranzulí	6.60 ± 0.15[§§]	bio	650[4]	Coranzulí	Seggiaro (1994)
Panizos	6.79 ± 0.02	bio	650[5]	Panizos	This study
Yerbas Buenas	8.30 ± 0.04	bio	N.D.	N.D.	This study
Sifon	8.33 ± 0.06	bio	1000[1]	N.D.	This study
Chaxas I	8.35 ± 0.03	bio	N.D.	N.D.	This study
Vilama	8.41 ± 0.02	bio	1400[6]	Vilama	This study
Artola	9.40 ± 0.03	bio	>100	N.D.	This study
Granada	Ca. 9.8	bio	60[7]	Abra Granada	Caffe et al. (2008)
Divisoco	10.18 ± 0.15	bio	N.D.	N.D.	This study
Lower Rio San Pedro	10.71 ± 0.14	bio	>100	Carcanal	This study
Pairique complex	11–10	bio	<10[7]	N.D.	Caffe et al. (2008)

Note: As shown in this study, K-Ar ages and unconstrained volume calculations should be approached with caution. All ages are $^{40}Ar/^{39}Ar$ except for those marked with [§] (relative age), and [§§] (K-Ar age).

*Mineral used to calculate age (bio—biotite, san—sanidine, plag—plagioclase).

†Volumes calculated in this study are dense rock equivalent (DRE) except where noted ([1]de Silva, 1989b; [2]Schmitt et al., 2001; [3]Lindsay et al., 2001a; [4]Seggiaro,1994; [5]Ort, 1993; [6]maximum estimate of Soler et al., 2007; [7]Caffe et al., 2008).

#N.A.—not applicable.

**N.D.—not determined.

strong chemical resemblance to Altiplano-Puna volcanic complex ignimbrites, such as the ca. 100 ka Chao dacite in northern Chile (de Silva et al., 1994) and the 89–94 ka Chascon-Runtu Jarita dome complex in Bolivia (Watts et al., 1999), represents the most recent felsic eruptions within the Altiplano-Puna volcanic complex (Fig. 9G).

The overall spatiotemporal trend of Altiplano-Puna volcanic complex volcanism lacks a dominant east-west sweeping trend that might be expected from a progressively steepening subducting slab (Kay and Coira, 2009), although the earliest eruptions of small stocks and domes did occur in the eastern reaches of the Altiplano-Puna volcanic complex (Kussmaul et al., 1975; Caffe et al., 2002). Ignimbrite volcanism was initially widespread and shows a consistently wide footprint throughout much of the duration of the complex. Such a pattern is consistent with the thick crust of the Central Andes, which likely prevented the ascent of small volumes of magma. Babeyko et al. (2002) used thermo-mechanical modeling to argue that delamination of dense lower lithosphere likely generated the large volumes of mantle magmas capable of thermally maturing the crust and producing the immense crust-rich ignimbrites of the Altiplano-Puna volcanic complex in the 10–20 m.y. following tectonic shortening. The spatiotemporal pattern and the high crustal temperatures required for the numerous large, caldera-forming eruptions (de Silva et al., 2006a) are also consistent with a major heat-producing event, such as lithospheric delamination, which has also been argued elsewhere in the Central Andes (e.g., Kay and Kay, 1993; Kay et al., 1994; Garzione et al., 2006). Data from recent seismic studies (Schurr et al., 2006; Heit et al., 2008) support this conclusion, as they appear to show delaminated lithospheric blocks sinking beneath the Altiplano-Puna volcanic complex as well as large, low-velocity regions concentrated in the eastern portion of the Altiplano-Puna volcanic complex. Current surface uplift by magmatic inflation beneath Uturuncu volcano (Pritchard and Simons, 2004) has also been suggested as a possible location for a future supervolcanic eruption (Sparks et al., 2008).

Comparison to Other Large Silicic Volcanic Fields

The pattern of volcanism defined in the Altiplano-Puna volcanic complex and shown in Figure 10 is reminiscent of other large silicic volcanic fields, most notably the Southern Rocky Mountain volcanic field (Lipman, 2007) and the Southwestern Nevada volcanic field (Sawyer et al., 1994) of the United States. Each of these three silicic centers is characterized by pulses with eruption rates that are much higher than the long-term average of the volcanic field, and each has an eruptive history lasting 8–13 m.y. (Fig. 10). The peak eruption rates and intensity of the most productive pulses in the Altiplano-Puna volcanic complex are also similar to the eruptive flux during the past two million years at Yellowstone and Taupo (Houghton et al., 1995). As noted by Lipman and McIntosh (2008), both the Altiplano-Puna volcanic complex and the Southern Rocky Mountain volcanic field are underlain by regional gravity lows that are suggestive of mid- to upper-crustal batholiths. Lipman (2007)

and de Silva and Gosnold (2007) have argued that the pulsing eruptive history of the Southern Rocky Mountain volcanic field and the Altiplano-Puna volcanic complex is suggestive of episodic, or incremental, assembly of these respective Cordilleran batholiths. This hypothesis comes at the heels of many recent studies of plutonic complexes that suggest individual plutonic bodies are themselves constructed incrementally over durations of hundreds of thousands to a few million years (Coleman et al., 2004; Matzel et al., 2006; Walker et al., 2007; Schaltegger et al., 2009). The nested caldera complexes of the Altiplano-Puna volcanic complex may also reflect such processes, as the multimillion-year longevity and periodic eruption history of these complexes is likely sustained through repeated magmatic injections. Successive VEI 8 eruptions with recurrences of 2.6, 2.2, and 1.6 m.y. at the Pastos Grandes, Guacha, and La Pacana caldera complexes, respectively, suggest that plutons beneath these centers may be assembled over hundreds of thousands to millions of years in this region of thick continental crust.

Many smaller eruptive centers show similar durations and volume-time patterns of volcanism to the large silicic volcanic complexes (see compilation in Grunder et al., 2008). In the case of the ~350 km^3 Aucanquilcha volcanic cluster, located along the modern arc front along the western border of the Altiplano-Puna volcanic complex, the volume-time relations and the centralization of eruptions mirror that of the Altiplano-Puna volcanic complex, suggesting an interplay between the Altiplano-Puna volcanic complex magmatic system and the frontal arc volcanism (Babeyko et al., 2002; Grunder et al., 2008). Further investigation is needed to determine the link between these two magmatic systems.

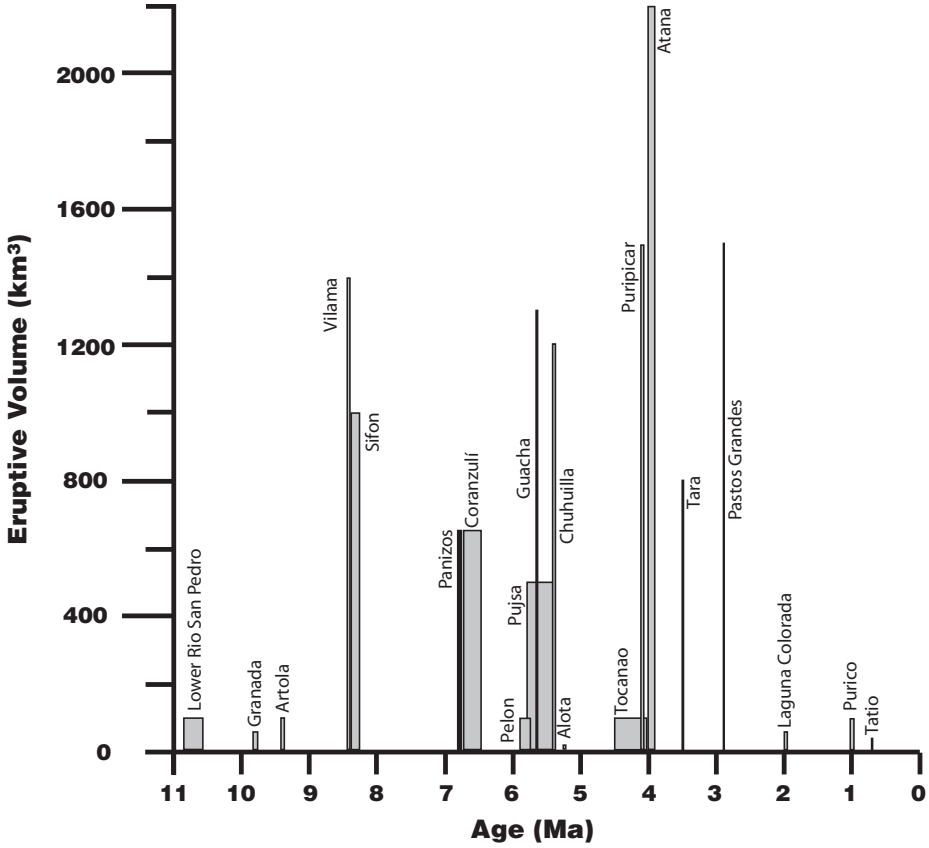

Figure 8. Volume-time relations of Altiplano-Puna volcanic complex ignimbrites. Horizontal width of each unit is ±2σ of the preferred age of each unit listed in Table 5.

TABLE 6. ERUPTION RATES OF ALTIPLANO-PUNA VOLCANIC COMPLEX IGNIMBRITE VOLCANISM

	Age (Ma)	Volume (km^3)	Duration (k.y.)	Eruption rate (km^3/k.y.)	Ignimbrites used in calculations
A	11.0–9.0	280	2000	0.14	Pairique, Cortadera, LRSP, Granada, Artola
B	9.0–7.5	2400	1500	1.60	Vilama, Sifon
C	7.5–6.0	1300	1500	0.87	Panizos, Coranzulí
D	6.0–4.5	3120	1500	2.08	Pelon, Pujsa, Guacha, Chuhuilla, Alota
E	4.5–3.0	4000	1500	2.67	Tocanao, Puripicar, Atana, Tara
F	3.0–1.5	1570	1500	1.05	Pastos Grandes, Laguna Colorada, Puripica Chico
G	1.5–0	150	1500	0.10	Purico, Tatio, Filo Delgado
H	11.0–0	12,820	11,000	1.17	All listed above
Ignimbrite pulses					
Pulse 1	8.41–8.33	2400	80	30.00	Sifon, Vilama
Pulse 2	5.60–5.45	3000	150	20.00	Pujsa, Guacha, Chuhuilla
Pulse 3	4.06–3.96	3100	100	31.00	Puripicar, Atana
Pulse 3a	4.06–3.49	3900	570	6.84	Puripicar, Atana, Tara
Pulse 3b	4.06–2.89	5400	1170	4.62	Puripicar, Atana, Tara, Pastos Grandes

Note: Letters A–H match ignimbrite distribution diagrams of Figure 9. LRSP—Lower Rio San Pedro.

CONCLUSIONS

High-precision $^{40}Ar/^{39}Ar$ geochronology, combined with new field, geochemical, and geophysical data provide the first comprehensive characterization of four newly described super-

Figure 9. Spatiotemporal patterns of volcanism in the Altiplano-Puna volcanic complex showing approximate locations of calderas (stippled lines) and estimated distributions of ignimbrites (outlines). Early ignimbrite volcanism (11.0–9.0 Ma) and the onset of major-caldera–forming volcanism (9.0–7.5 Ma) occurred in both the western and eastern reaches of the Altiplano-Puna volcanic complex. A second major ignimbrite pulse was initiated ca. 5.6 Ma with eruptions from Pastos Grandes, Guacha, and La Pacana caldera complexes. The most voluminous phase of volcanism (4.5–3.0 Ma) was focused near ~23°S. Note that the minor Talabre and Tuyajto ignimbrites plot south of the extent shown and that the majority of the Coranzulí ignimbrites plot east of the figure. The apparent gap in the composite record along the Bolivia-Chile border represents cover from the modern volcanic arc. See Table 6 for ignimbrite eruption rates corresponding to each time interval.

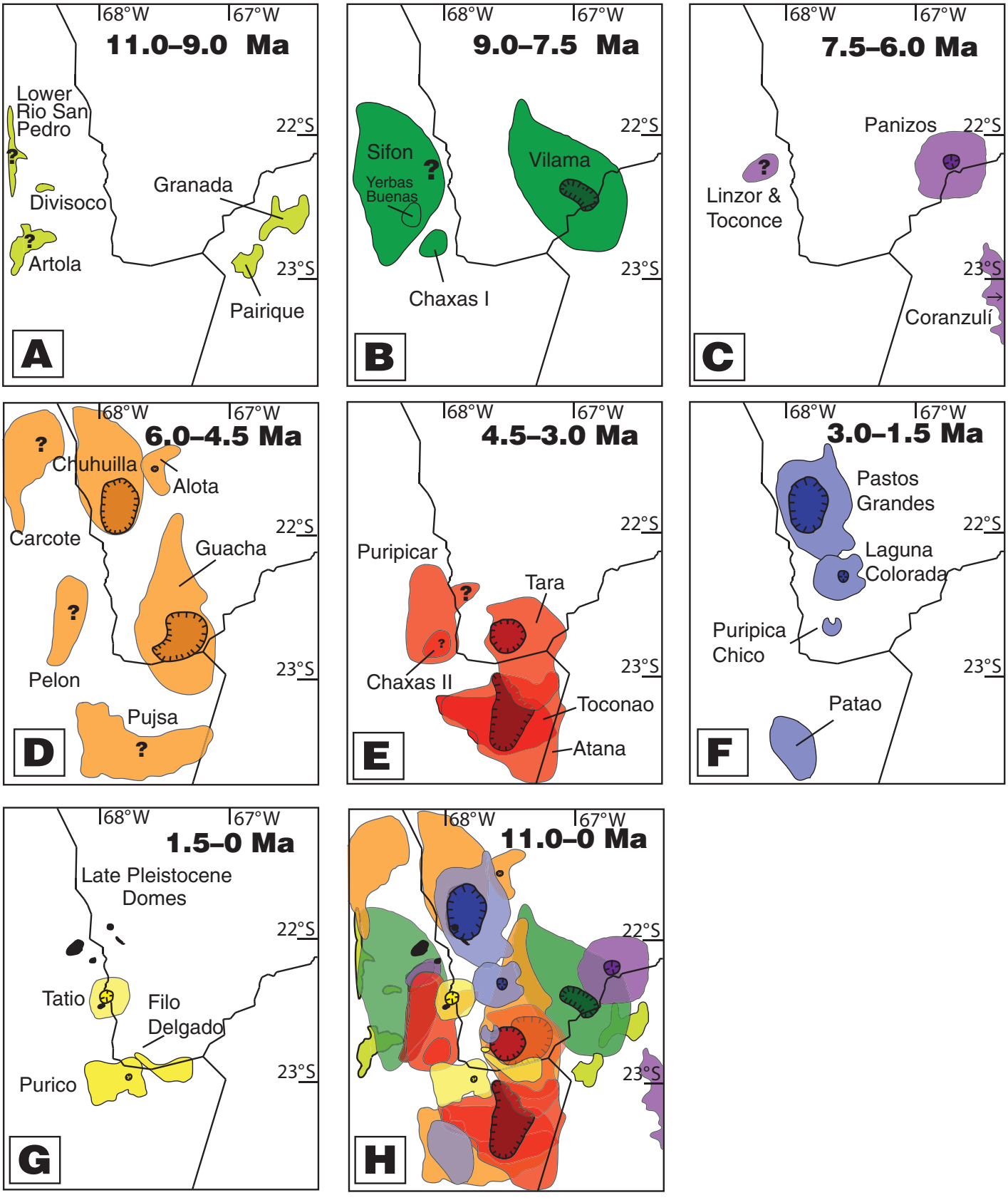

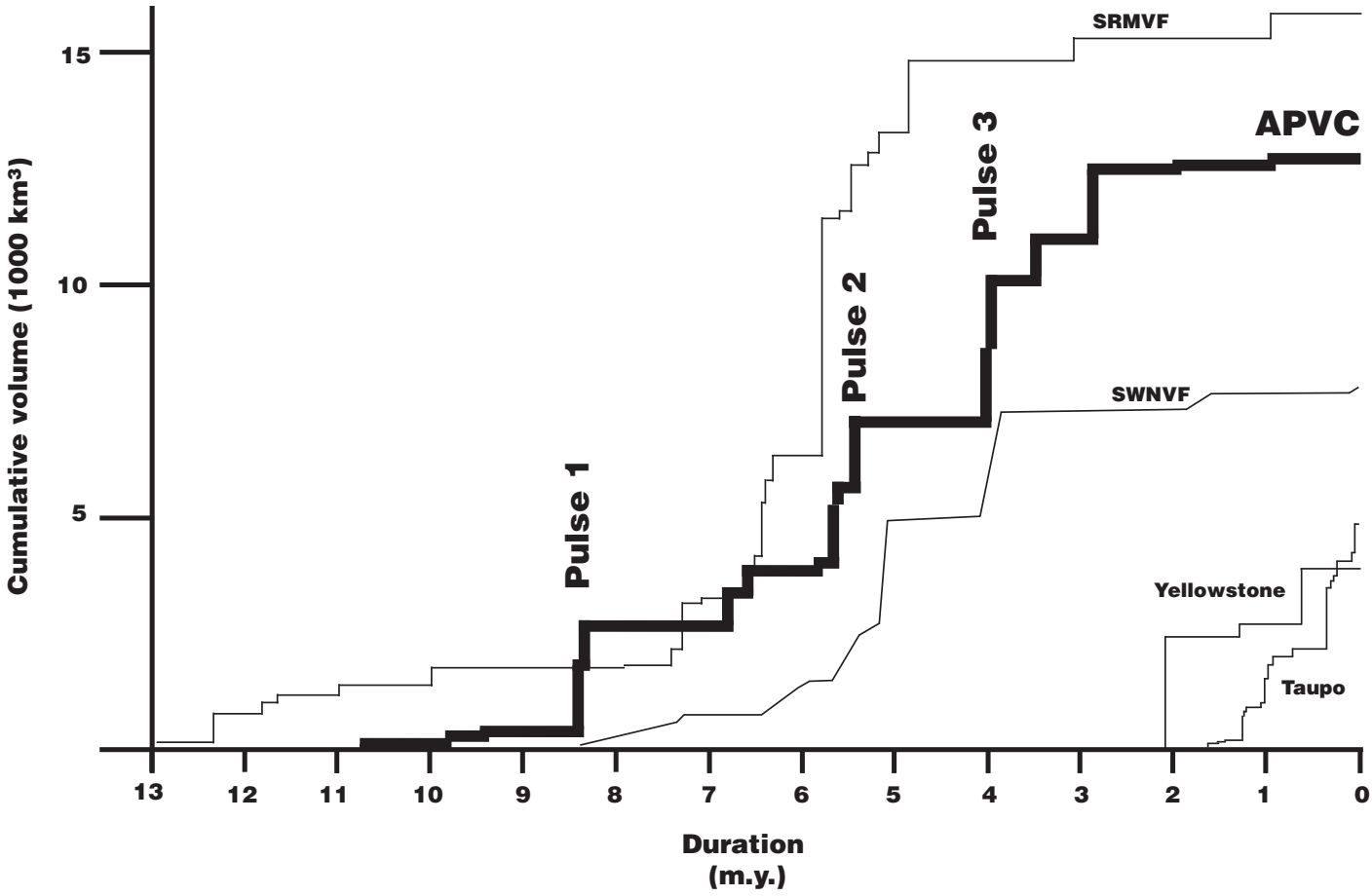

Figure 10. Cumulative volume versus time for ignimbrite eruptions in the Altiplano-Puna volcanic complex (APVC; thick line). Shown for comparison are the Southern Rocky Mountain (SRMVF; Lipman and McIntosh, 2008); Southwest Nevada (SWNVF; Sawyer et al., 1994); Yellowstone (Christiansen, 2001); and Taupo (Houghton et al., 1995) volcanic fields. Altiplano-Puna volcanic complex ignimbrite volcanism shows a distinct beginning at ca. 11 Ma, followed by waxing volcanism that is punctuated by three discrete pulses, and apparent waning during the last 3 m.y.

eruptions from the Pastos Grandes and Guacha caldera complexes of the Altiplano Puna volcanic complex of the Central Andes. The areal extents of the Chuhuilla, Guacha, Tara, and Pastos Grandes ignimbrites are each estimated to cover thousands of square kilometers and have volumes in excess of 800 km^3 DRE. These data, combined with previous Altiplano-Puna volcanic complex studies and the smaller eruptions described in this study, allow a comprehensive characterization of the volcanic complex. Overall, the eruption rate of the Altiplano-Puna volcanic complex averages 1.11 km^3/k.y., and is punctuated by three distinct eruptive pulses at ca. 8.4, ca. 5.5, and ca. 4.0 Ma, during which eruption rates increased dramatically to between 20 and 31 km^3/k.y. over durations from 80 to 150 k.y. The average and peak eruption rates are comparable to that of the Southern Rocky Mountain and Southwestern Nevada volcanic fields of the North American Cordillera, and are consistent with piecemeal construction of Cordilleran batholiths by incremental pulses of magmatism. The cyclic nature of individual caldera complexes implied by our geochronologic data support the hypothesis that individual plutons are also constructed incrementally. The ~10 m.y. duration of the Altiplano-Puna volcanic complex is also similar to the duration at the nearby Aucanquilcha volcanic cluster, as well as numerous other examples from the volcanic and plutonic record. Lithospheric removal provides a valid explanation for the high power rates implied by Altiplano-Puna complex volcanism as well as the high surface elevations and spatiotemporal trends of ignimbrite eruptions. Despite the apparent waning of Altiplano-Puna volcanic complex ignimbrite activity, the tendency for ignimbrite eruptions to occur in pulses, together with evidence for a still molten portion of melt beneath the complex, suggests that the Altiplano-Puna volcanic complex remains capable of producing large ignimbrites like those characterized in this study. Our findings provide a foundation for more focused field and petrologic research on the large silicic systems within the Bolivian Altiplano-Puna volcanic complex.

ACKNOWLEDGMENTS

This work was made possible by National Science Foundation (NSF) grants EAR-0710545 and EAR-0538159. The authors would like to thank Victor Ramirez, Victor Quispe, Paola Ballon, Wilber Acarapi, Lidia Nina, and Eugenio Roque for their assistance in the field; and Xifan Xang and John Hora for analytical assistance at the University of Wisconsin–Madison Rare Gas Geochronology Laboratory. We would also like to thank Lee Powell, whose talent and dedication led to automation of the $^{40}Ar/^{39}Ar$ analytical system, critical to this study; and Miguel Garcés and Bet Beamud at the paleomagnetism laboratory at the Instituto Jaume Almera, University of Barcelona, for their hospitality. de Silva is indebted to Ing. Raul Carrasco for his guidance in the study area in 1988. We also thank Susanne Mahlburg Kay and an anonymous reviewer for helpful critical reviews.

REFERENCES CITED

Allmendinger, R.W., Jordan, T.E., Kay, S.M., and Isacks, B.L., 1997, The evolution of the Altiplano-Puna plateau of the Central Andes: Annual Review of Earth and Planetary Sciences, v. 25, p. 139–174, doi: 10.1146/annurev.earth.25.1.139.

Almendras, O., and Baldellón, E., 1997, Hoja Ollague/San Agustin 5930/6030: Servicio Nacional de Geológica y Mineria Carta Geológica de Bolivia Publicacíon SGM Serie I–CGB-49, scale 1:100,000, 1 sheet.

Almendras, O., García, H., and Baldellón, E., 1996, Hoja Laguan Busch/Intihuasi 6126/6226: Servicio Nacional de Geológica y Mineria Carta Geológica de Bolivia Publicacíon SGM Serie I–CGB-42, scale 1:100,000, 1 sheet.

Babeyko, A.Y., Sobolev, S.V., Trumbull, R.B., Oncken, O., and Lavier, L.L., 2002, Numerical models of crustal scale convection and partial melting beneath the Altiplano-Puna plateau: Earth and Planetary Science Letters, v. 199, no. 3–4, p. 373–388, doi: 10.1016/S0012-821X(02)00597-6.

Bailey, J.E., Self, S., Wooller, L.K., and Mouginis-Mark, P.J., 2007, Discrimination of fluvial and eolian features on large ignimbrite sheets around La Pacana caldera, Chile, using Landsat and SRTM-derived DEM: Remote Sensing of Environment, v. 108, no. 1, p. 24–41, doi: 10.1016/j.rse.2006.10.018.

Baker, M.C.W., 1977, Geochronology of Upper Tertiary volcanic activity in the Andes of north Chile: International Journal of Earth Sciences, v. 66, no. 1, p. 455–465.

Baker, M.C.W., 1981, The nature and distribution of Upper Cenozoic ignimbrite centers in the Central Andes: Journal of Volcanology and Geothermal Research, v. 11, p. 293–315, doi: 10.1016/0377-0273(81)90028-7.

Baker, M.C.W., and Francis, P.W., 1978, Upper Cenozoic volcanism in the Central Andes—Ages and volume: Earth and Planetary Science Letters, v. 41, no. 2, p. 175–187, doi: 10.1016/0012-821X(78)90008-0.

Barquero-Molina, M., 2003, $^{40}Ar/^{39}Ar$ Chronology and Paleomagnetism of Ignimbrites and Lavas from the Central Volcanic Zone, Northern Chile, and $^{40}Ar/^{39}Ar$ Chronology of Silicic Ignimbrites from Honduras and Nicaragua [MS thesis]: Madison, University of Wisconsin, 70 p.

Caffe, P.J., Trumbull, R.B., Coira, B.L., and Romer, R.L., 2002, Petrogenesis of early Neogene magmatism in the northern Puna: Implications for magma genesis and crustal processes in the Central Andean Plateau: Journal of Petrology, v. 43, no. 5, p. 907–942, doi: 10.1093/petrology/43.5.907.

Caffe, P.J., Soler, M.M., Coira, B.L., Onoe, A.T., and Cordani, U.G., 2008, The Granada ignimbrite: A compound pyroclastic unit and its relationship with Upper Miocene caldera volcanism in the northern Puna: Journal of South American Earth Sciences, v. 25, p. 464–484, doi: 10.1016/j.jsames.2007.10.004.

Chmielowski, J., Zandt, G., and Haberland, C., 1999, The Central Andean Altiplano-Puna magma body: Geophysical Research Letters, v. 26, no. 6, p. 783–786, doi: 10.1029/1999GL900078.

Choque, N., Ramírez, V.F., and Pocoaca, G.R., 1996, Hoja Volcán Putana 6026: Servicio Nacional de Geológica y Mineria Carta Geológica de Bolivia Publicacíon SGM Serie I–CGB-41, scale 1:100,000, 1 sheet.

Christiansen, R.L., 2001, The Quaternary and Pliocene Yellowstone Plateau Volcanic Field of Wyoming, Idaho, and Montana: U.S. Geological Survey Professional Paper 729-G, 145 p.

Coleman, D.S., Gray, W., and Glazner, A.F., 2004, Rethinking the emplacement and evolution of zoned plutons: Geochronologic evidence for incremental assembly of the Tuolumne Intrusive Suite, California: Geology, v. 32, no. 5, p. 433–436, doi: 10.1130/G20220.1.

de Silva, S.L., 1987, Large volume explosive silicic volcanism in the Central Andes of North Chile [Ph.D. thesis]: Milton Keynes, UK, Open University, 409 p.

de Silva, S.L., 1989a, Altiplano-Puna volcanic complex of the Central Andes: Geology, v. 17, p. 1102–1106, doi: 10.1130/0091-7613(1989)017<1102:APVCOT>2.3.CO;2.

de Silva, S.L., 1989b, Geochronology and stratigraphy of the ignimbrites from the 21°30′S to 23°30′S portion of the Central Andes of northern Chile: Journal of Volcanology and Geothermal Research, v. 37, p. 93–131.

Davidson, J.P., and de Silva, S.L., 1992, Volcanic rocks from the Bolivian Altiplano: Insights into crustal structure, contamination, and magma genesis in the Central Andes: Geology, v. 20, p. 1127–1130, doi: 10.1130/0091-7613(1992)020<1127:VRFTBA>2.3.CO;2.

Davidson, J.P., Harmon, R.S., and Wörner, G., 1991, The source of Central Andean magmas; some considerations, *in* Harmon, R.S., and Rapela, C.W., eds., Andean magmatism and its tectonic setting: Geological Society of America Special Paper 265, p. 233–243.

de Silva, S.L., and Francis, P.W., 1989, Correlation of large volume ignimbrites—Two case studies from the Central Andes of N. Chile: Journal of Volcanology and Geothermal Research, v. 37, no. 2, p. 133–149, doi: 10.1016/0377-0273(89)90066-8.

de Silva, S.L., and Francis, P.W., 1991, Volcanoes of the Central Andes: Berlin, Springer-Verlag, p. 1–216.

de Silva, S.L., and Gosnold, W.D., 2007, Episodic construction of batholiths: Insights from the spatiotemporal development of an ignimbrite flare-up: Journal of Volcanology and Geothermal Research, v. 167, no. 1–4, p. 320–335, doi: 10.1016/j.jvolgeores.2007.07.015.

de Silva, S.L., Self, S., Francis, P.W., Drake, R.E., and Ramirez, C.R., 1994, Effusive silicic volcanism in the Central Andes: The Chao dacite and other young lavas of the Altiplano-Puna volcanic complex: Journal of Geophysical Research, v. 99, no. B9, p. 17,805–17,825, doi: 10.1029/94JB00652.

de Silva, S.L., Zandt, G., Trumbull, R., and Viramonte, J., 2006a, Large-scale silicic volcanism—The result of thermal maturation of the crust, *in* Chen, Y.-T., and Ip, W.-H., eds., Advances in Geosciences: Singapore, World Scientific Press, p. 215–230.

de Silva, S., Zandt, G., Trumbull, R., Viramonte, J., Salas, G., and Jimenez, N., 2006b, Large ignimbrite eruptions and volcano-tectonic depressions in the Central Andes: A thermomechanical perspective, *in* de Natale, G., Troise, C., and Kilburn, C., eds., Mechanisms of activity and unrests at large caldera: Geological Society of London Special Publication 269, p. 47–63.

de Silva, S.L., Bailey, J.E., Mandt, K.E., and Viramonte, J.M., 2010, Yardangs in terrestrial ignimbrites: Synergistic remote and field observations on Earth with applications to Mars: Planetary and Space Science, v. 58, no. 4, p. 459–471, doi: 10.1016/j.pss.2009.10.002.

Fernández, S., Thompson, C., and Mamani, H., 1996, Hoja Volcán Juriques 6025: Servicio Nacional de Geológica y Mineria Carta Geológica de Bolivia Publicacíon SGM Serie I–CGB-46, scale 1:100,000, 1 sheet.

Folkes, C.B., Wright, H.W., Cas, R.A.F., de Silva, S.L., Lesti, C., and Viramonte, J.G., 2010, A re-appraisal of the stratigraphy and volcanology of the Cerro Galan volcanic system, NW Argentina: Bulletin of Volcanology (in press).

García, R., 1996, Hoja Laguna Corante/Picalto 6227/6327: Servicio Nacional de Geológica y Mineria Carta Geológica de Bolivia Publicacíon SGM Serie I–CGB-48, scale 1:100,000, 1 sheet.

Gardeweg, M., and Ramírez, C.F., 1987, La Pacana caldera and the Atana ignimbrite—A major ash-flow and resurgent caldera complex in the Andes of northern Chile: Bulletin of Volcanology, v. 49, no. 3, p. 547–566, doi: 10.1007/BF01080449.

Garzione, C.N., Molnar, P., Libarkin, J.C., and MacFadden, B.J., 2006, Rapid late Miocene rise of the Bolivian Altiplano: Evidence for removal of mantle lithosphere: Earth and Planetary Science Letters, v. 241, p. 543–556, doi: 10.1016/j.epsl.2005.11.026.

Grunder, A.L., Klemetti, E.W., Feeley, T.C., and McKee, C.M., 2008, Eleven million years of arc volcanism at the Aucanquilcha volcanic cluster, northern Chilean Andes: Implications for the life span and emplacement of plutons: Transactions of the Royal Society of Edinburgh–Earth Sciences, v. 97, p. 415–436.

Guest, J.E., 1969, Upper Tertiary ignimbrites in the Andean Cordillera of part of the Antofagasta province, northern Chile: Geological Society of America Bulletin, v. 80, p. 337–362, doi: 10.1130/0016-7606(1969)80[337:UTIITA]2.0.CO;2.

Heit, B., Koulakov, I., Asch, G., Yuan, X., Kind, R., Alcocer-Rodriguez, I., Tawackoli, S., and Wilke, H., 2008, More constraints to determine the seismic structure beneath the Central Andes at 21°S using teleseismic tomography analysis: Journal of South American Earth Sciences, v. 25, p. 22–36.

Hildreth, W., 1981, Gradients in silicic magma chambers: Implications for lithospheric magmatism: Journal of Geophysical Research, v. 86, p. 10,153–10,192, doi: 10.1029/JB086iB11p10153.

Hildreth, W., and Mahood, G., 1985, Correlation of ash-flow tuffs: Geological Society of America Bulletin, v. 96, p. 968–974, doi: 10.1130/0016-7606(1985)96<968:COAT>2.0.CO;2.

Hora, J.M., Singer, B.S., Jicha, B.R., Beard, B.L., Johnson, C.M., de Silva, S.L., and Salisbury, M.J., 2010, Volcanic biotite-sanidine $^{40}Ar/^{39}Ar$ age discordances reflect Ar partitioning and pre-eruption closure in biotite: Geology, v. 38, p. 923–926, doi:10.1130/G31064.1.

Houghton, B.F., Wilson, C.J.N., McWilliams, M.O., Lanphere, M.A., Weaver, S.D., Briggs, R.M., and Pringle, M.S., 1995, Chronology and dynamics of a large silicic magmatic system: Central Taupo volcanic zone, New Zealand: Geology, v. 23, no. 1, p. 13–16, doi: 10.1130/0091-7613(1995)023<0013:CADOAL>2.3.CO;2.

Isacks, B.L., 1988, Uplift of the Central Andean Plateau and bending of the Bolivian orocline: Journal of Geophysical Research, v. 93, p. 3211–3231, doi: 10.1029/JB093iB04p03211.

Johnson, D.M., Hooper, P.R., and Conrey, R.M., 1999, XRF analysis of rocks and minerals for major and trace elements on a single low-dilution Li-tetraborate fused bead: Advances in X-Ray Analysis, v. 41, p. 117–132.

Kay, R.M., and Kay, S.M., 1993, Delamination and delamination magmatism: Tectonophysics, v. 219, no. 1–3, p. 177–189, doi: 10.1016/0040-1951(93)90295-U.

Kay, S.M., and Coira, B.L., 2009, Shallowing and steepening subduction zones, continental lithospheric loss, magmatism, and crustal flow under the Central Andean Altiplano-Puna plateau, *in* Kay, S.M., Ramos, V.A., and Dickinson, W.R., eds., Backbone of the Americas: Shallow Subduction, Plateau Uplift, and Ridge and Terrane Collision: Geological Society of America Memoir 204, p. 229–259, doi: 10.1130/2009.1204(11).

Kay, S.M., Coira, B., and Viramonte, J., 1994, Young mafic back-arc volcanic rocks as guides to lithospheric delamination beneath the Argentine Puna plateau, Central Andes: Journal of Geophysical Research, v. 99, p. 24,323–24,339, doi: 10.1029/94JB00896.

Kelley, S., 2002, Excess argon in K-Ar and Ar-Ar geochronology: Chemical Geology, v. 188, no. 1–2, p. 1–22, doi: 10.1016/S0009-2541(02)00064-5.

Kussmaul, S., Jordan, L., and Ploskonka, E., 1975, Isotopic ages of Tertiary volcanic rocks of SW-Bolivia: Geologisches Jahrbuch (Hannover), v. B14, p. 111–120.

Lahsen, A., 1982, Upper Cenozoic volcanism and tectonism in the Andes of northern Chile: Earth-Science Reviews, v. 18, p. 285–302, doi: 10.1016/0012-8252(82)90041-1.

Lema, J., and Ramos, W., 1996, Hoja Sanabria 6027: Servicio Nacional de Geológica y Mineria Carta Geológica de Bolivia Publicacíon SGM Serie I–CGB-43, scale 1:100,000, 1 sheet.

Lindsay, J.M., de Silva, S., Trumbull, R., Emmermann, R., and Wemmer, K., 2001a, La Pacana caldera, N. Chile: A re-evaluation of the stratigraphy and volcanology of one of the world's largest resurgent calderas: Journal of Volcanology and Geothermal Research, v. 106, no. 1–2, p. 145–173, doi: 10.1016/S0377-0273(00)00270-5.

Lindsay, J.M., Schmitt, A.K., Trumbull, R.B., de Silva, S.L., Siebel, W., and Emmermann, R., 2001b, Magmatic evolution of the La Pacana caldera system, Central Andes, Chile: Compositional variation of two cogenetic, large-volume felsic ignimbrites: Journal of Petrology, v. 42, no. 3, p. 459–486, doi: 10.1093/petrology/42.3.459.

Lipman, P.W., 2007, Incremental assembly and prolonged consolidation of Cordilleran magma chambers: Evidence from the Southern Rocky Mountain volcanic field: Geosphere, v. 3, no. 1, p. 42–70, doi: 10.1130/GES00061.1.

Lipman, P.W., and McIntosh, W.C., 2008, Colorado: Where did the ignimbrites come from? Eruptive and noneruptive

calderas, northeastern San Juan Mountains: Geological Society of America Bulletin, v. 120, no. 7, p. 771–795, doi: 10.1130/B26330.1.

Mason, B.G., Pyle, D.M., and Oppenheimer, C., 2004, The size and frequency of the largest explosive eruptions on Earth: Bulletin of Volcanology, v. 66, doi: 10.1007/s00445-004-0355-9.

Matzel, J.E.P., Bowring, S.A., and Miller, R.B., 2006, Time scales of pluton construction at differing crustal levels; examples from the Mount Stuart and Tenpeak intrusions, north Cascades, Washington: Geological Society of America Bulletin, v. 118, p. 1412, doi: 10.1130/B25923.1.

Newhall, C.G., and Self, S., 1982, The volcanic explosivity index (VEI): An estimate of explosive magnitude for historical volcanism: Journal of Geophysical Research, v. 87, p. 1231–1238, doi: 10.1029/JC087iC02p01231.

Ort, M.H., 1993, Eruptive processes and caldera formation in a nested downsag collapse caldera: Cerro Panizos, Central Andes Mountains: Journal of Volcanology and Geothermal Research, v. 56, p. 221–252, doi: 10.1016/0377-0273(93)90018-M.

Ort, M.H., Coira, B.L., and Mazzoni, M.M., 1996, Generation of a crust-mantle magma mixture: Magma sources and contamination at Cerro Panizos, Central Andes: Contributions to Mineralogy and Petrology, v. 123, no. 3, p. 308–322, doi: 10.1007/s004100050158.

Pacheco, J., and Ramírez, V., 1996, Hoja Queteña 6127: Servicio Nacional de Geológica y Mineria Carta Geológica de Bolivia Publicacíon SGM Serie I–CGB-40, scale 1:100,000, 1 sheet.

Pacheco, J., and Ramírez, V., 1997a, Hoja Geológica Cañapa/Alota 5929/6029: Servicio Nacional de Geológica y Mineria Carta Geológica de Bolivia Publicacíon SGM Serie I–CGB-45, scale 1:100,000, 1 sheet.

Pacheco, J., and Ramírez, V., 1997b, Hoja Geológica Soniquera 6128: Servicio Nacional de Geológica y Mineria Carta Geológica de Bolivia Publicacíon SGM Serie I–CGB-51, scale 1:100,000, 1 sheet.

Pritchard, M.E., and Simons, M., 2004, An InSAR-based survey of volcanic deformation in the Central Andes: Geochemistry, Geophysics, Geosystems, v. 5, doi: 10.1029/2003GC000610.

Renne, P.R., Swisher, C.C., Deino, A.L., Karner, D.B., Owens, T.L., and DePaolo, D.J., 1998, Intercalibration of standards, absolute ages and uncertainties in $^{40}Ar/^{39}Ar$ dating: Chemical Geology, v. 145, p. 117–152, doi: 10.1016/S0009-2541(97)00159-9.

Sawyer, D.A., Fleck, R.J., Lanphere, M.A., Warren, R.G., Broxton, D.E., and Hudson, M.R., 1994, Episodic caldera volcanism in the Miocene southwestern Nevada volcanic field: Revised stratigraphic framework, $^{40}Ar/^{39}Ar$ geochronology, and implications for magmatism and extension: Geological Society of America Bulletin, v. 106, p. 1304–1318, doi: 10.1130/0016-7606(1994)106<1304:ECVITM>2.3.CO;2.

Schaltegger, U., Brack, P., Ovtcharova, M., Peytcheva, I., Schoene, B., Stracke, A., Marocchi, M., and Bargossi, G.M., 2009, Zircon and titanite recording 1.5 million years of magma accretion, crystallization and initial cooling in a composite pluton (southern Adamello batholith, northern Italy): Earth and Planetary Science Letters, v. 286, no. 1–2, p. 208–218, doi: 10.1016/j.epsl.2009.06.028.

Schmitt, A.K., de Silva, S.L., Trumbull, R.B., and Emmermann, R., 2001, Magma evolution in the Purico ignimbrite complex, northern Chile: Evidence for zoning of a dacitic magma by injection of rhyolitic melts following mafic recharge: Contributions to Mineralogy and Petrology, v. 140, no. 6, p. 680–700.

Schurr, B., Rietbrock, A., Asch, G., Kind, R., and Oncken, O., 2006, Evidence for lithospheric detachment in the central Andes from local earthquake tomography: Tectonophysics, v. 415, p. 203–223, doi: 10.1016/j.tecto.2005.12.007.

Seggiaro, R.E., 1994, Petrología, Geoquímica y Mecanismos de Erupción del Complejo Volcánico Coranzulí [Ph.D. thesis]: Salta, Argentina, Universidad Nacional de Salta, 137 p.

Seggiaro, R.E., and Aniel, B., 1989, Los ciclos piroclásticos del área Tiomayo-Coranzulí, Provincia de Jujuy: Asociación Geológica Argentina Revista, v. 44, p. 394–401.

Self, S., 2006, The effects and consequences of very large explosive volcanic eruptions: Philosophical Transactions of the Royal Society of London, v. 364, p. 2073–2097, doi: 10.1098/rsta.2006.1814.

Singer, B.S., Ackert, R.P., and Guillou, H., 2004, $^{40}Ar/^{39}Ar$ and K-Ar chronology of Pleistocene glaciations in Patagonia: Geological Society of America Bulletin, v. 116, no. 3, p. 434–450, doi: 10.1130/B25177.1.

Smith, M.E., Singer, B., and Carroll, A., 2003, $^{40}Ar/^{39}Ar$ geochronology of the Eocene Green River Formation, Wyoming: Geological Society of America Bulletin, v. 115, no. 5, p. 549–565, doi: 10.1130/0016-7606(2003)115<0549:AGOTEG>2.0.CO;2.

Soler, M.M., Caffe, P.J., Coira, B.L., Onoe, A.T., and Kay, S.M., 2007, Geology of the Vilama caldera: A new interpretation of a large-scale explosive event in the Central Andean plateau during the Upper Miocene: Journal of Volcanology and Geothermal Research, v. 164, no. 1–2, p. 27–53, doi: 10.1016/j.jvolgeores.2007.04.002.

Sparks, R.S.J., Self, S., Grattan, J.P., Oppenheimer, C., Pyle, D.M., and Rymer, H., 2005, Super-Eruptions: Global Effects and Future Threats: Report of a Geological Society of London Working Group: London, UK, Geological Society of London, 24 p.

Sparks, S.J., Folkes, C.B., Humphreys, M., Barford, D.N., Clavero, J., Sunagua, M.L., McNutt, S.R., and Pritchard, M.E., 2008, Uturuncu volcano, Bolivia: Volcanic unrest due to mid-crustal magma intrusion: American Journal of Science, v. 308, p. 727–769, doi: 10.2475/06.2008.01.

Strecker, M.R., Alonso, R.N., Bookhagen, B., Carrapa, B., Hilley, G.E., Sobel, E.R., and Trauth, M.H., 2007, Tectonics and Climate of the Southern Central Andes: Annual Review of Earth and Planetary Sciences, v. 35, p. 747–787.

Walker, B.A., Jr., Miller, C.F., Claiborne, L.L., Wooden, J.L., and Miller, J.S., 2007, Geology and geochronology of the Spirit Mountain batholith, southern Nevada: Implications for timescales and physical processes of batholith construction: Journal of Volcanology and Geothermal Research, v. 167, p. 239–262, doi: 10.1016/j.jvolgeores.2006.12.008.

Watts, R.B., de Silva, S.L., Jimenez, G., and Croudace, I.W., 1999, Effusive silicic volcanism triggered and fueled by recharge: A case study of the Cerro Chascon–Runtu Jarita complex of SW Bolivia: Bulletin of Volcanology, v. 61, p. 241–264, doi: 10.1007/s004450050274.

Wörner, G., Moorbath, S., Horn, S., Entenmann, J., Harmon, R.S., Davidson, J.P., and Lopez-Escobar, L., 1994, Large- and fine-scale geochemical variations along the Andean arc of northern Chile (17.5°–22°S), *in* Ruetter, K.J., Scheuber, E., and Wigger, P.J., eds., Tectonics of the Southern Central Andes; Structure and Evolution of an Active Continental Margin: Berlin, Germany, Springer-Verlag, p. 77–92.

Zandt, G., Leidig, M., Chmielowski, J., Baumont, D., and Yuan, X.H., 2003, Seismic detection and characterization of the Altiplano-Puna magma body, Central Andes: Pure and Applied Geophysics, v. 160, no. 3, p. 789–807, doi: 10.1007/PL00012557.

Manuscript Received 22 February 2010
Revised Manuscript Received 22 June 2010
Manuscript Accepted 19 July 2010

Printed in the USA